PREDICTING THE RELIABILITY OF PACKAGE-ON-PACKAGE-ON-PACKAGE (POPOP) INTERCONNECTIONS BASED ON ACCELERATED AGING EXPERIMENTS AND COMPUTATIONAL MODELING

P. T. Vianco, J.A. Rejent, J.M Grazier, A.C. Kilgo, B.M. McKenzie, and M.K. Neilsen Sandia National Laboratories Albuquerque, NM USA ptvianc@sandia.gov

ABSTRACT

Package-on-package (PoP) and package-onpackage-on-package (PoPoP) technologies are being considered to reduce the size, weight, and power (SWaP) of military, space, and satellite electronics. The long-term reliability of PoPoP solder joints was assessed under thermal mechanical fatigue (TMF). The study included accelerated aging experiments (-55°C/125°C temperature cycling) and development of a computational model. Data were analyzed using the two-parameter (2P) Weibull probability distribution (characteristic lifetime, η , and slope, β). Backwards compatible, test vehicles (bottom solder joints (SnPb paste/SAC305 solder balls) exhibited excellent TMF performance ($\eta =$ 2600 \pm 200 cycles; β = 7.6 \pm 3.5) as did the middle (n = 2500 ± 300 cycles; $\beta = 6.6\pm3.4$) and top joints (η = 2600 ± 200 cycles; $\beta = 8.7\pm4.0$). The 100% SAC305 test vehicle showed comparable η values: bottom joints, 2200±200 cycles; middle joints, 2600±500 cycles; and top joints, 2400±200 cycles. Underfill in the bottom gap *improved* the η of the SnPb/SAC305 interconnections but reduced that of the 100% SAC305 solder joints. When underfilled, the 100% SAC305 joints exhibited two failure modes: a "low η " mode that showed only TMF cracks and a "high n" mode that had both TMF and tensile cracks. The computational model predicted that PoPoP warpage was not significantly changed by underfill placed in the bottom gap. Initial quantitative predictions of N_f were less than satisfactory, requiring further development of the model for the latter be a suitable design tool.

Key words: Stacked packaging, PoPoP, reliability, modeling.

INTRODUCTION

The miniaturization of electronic packages, whether passive devices such as capacitors and resistors, or active devices ranging from diodes to microprocessors, has allowed a greater number of components to be assembled on printed circuit boards (PCBs). The benefit to the consumer electronics industry as well as for the high reliability electronics community (military, satellite, and space) has been, not only smaller, lighter products, but also systems with enhanced functionality [1].

The rapid growth of hand-held, personal electronics over the past ten years has forced product designers to reduce the footprint of area-array packages. Therefore, the only remaining dimension available to increase functionality was in the vertical ("z") direction, which has led to the development of three-dimensional (3-D) packaging.

Stacked packages are of greater interest to the highreliability electronics community. Stacked packaging refers to the mounting of molded packages upon one-another. The earliest renditions of stacked packages used peripherally leaded components [2]. This practice began by stacking gull-wing leaded components atop oneanother to increase the memory die available on the printed wiring assembly (PWA) [3]. Today, stacked packages are based primarily upon the area-array format that stacks ball-grid array (BGA) packages upon one-another. The two variants that can best accommodate the environments of highreliability electronics are package-on-package (PoP) and package-on-package (PoPoP). Although it is theoretically possible to stack a greater number of packages, components

have been limited to the PoP and PoPoP configurations due to manufacturing challenges as well as the reduced product thicknesses for consumer electronics. Also, the stacking count is restricted by component survivability under shock and vibration conditions that are often associated with high-reliability applications.

The reason that stacked packages have earned a greater interest to the high-reliability electronics community is derived from the known good die (KGD) concept that, in effect, has evolved into the "known good package" approach. packaging allows for verifying the performance and reliability of each individual package after burn-in, qualification, and acceptance testing. Individual package testing increases the likelihood of eliminating defects from it, which are responsible for infant mortality and latent failures. Subsequently, when the individual parts are assembled and mounted to the printed circuit board (PCB), the stacked package will have a high probability of demonstrating the required, longterm reliability performance. The need is minimized to rework or repair the printed wiring assembly (PWA) due the failure of a single package within the stacked component.

Stacked packaging has drawn the attention of Sandia National Laboratories for use in advanced electronic systems. The first phase of a multi-year evaluation of stacked package technology has considered the thermal mechanical fatigue (TMF) performance of PoP solder joints [4]. Empirical data were obtained from PoP test vehicles that were subjected to thermal cycling (-55°C/125°C; 10 min Their daisy chain circuits were hold times). monitored by event detectors per the IPC-9701A specification ("Performance Test Methods and Qualification Requirements for Surface Mount Solder Attachments," 2006, Assoc. Connecting Elect. Indus., Bannockburn, IL). An important goal of that study was to compare the reliability performance of second-level, Pb-free interconnections made with 96.5Sn-3.0Ag-0.5Cu (SAC305) solder balls and paste, to that of backwards compatible solder joints made with SAC305 solder balls and eutectic 63Sn-37Pb (wt.%, abbreviated SnPb) solder paste. Backwards

compatibility remains an important option for high-reliability electronics since many products are still being assembled with SnPb solder paste. As shown by the plot of cumulative failure fraction as a function of cycles to failure (N_f) in Fig. 1, the backwards compatible interconnections exhibited a slightly *better* reliability than the Pb-free solder joints formed of 100% SAC305 solder. This finding provided an impetus to investigate backward compatible interconnections for PoPoP assemblies, thereby enabling the implementation of the latter technology into a wider range of highend electronic products.

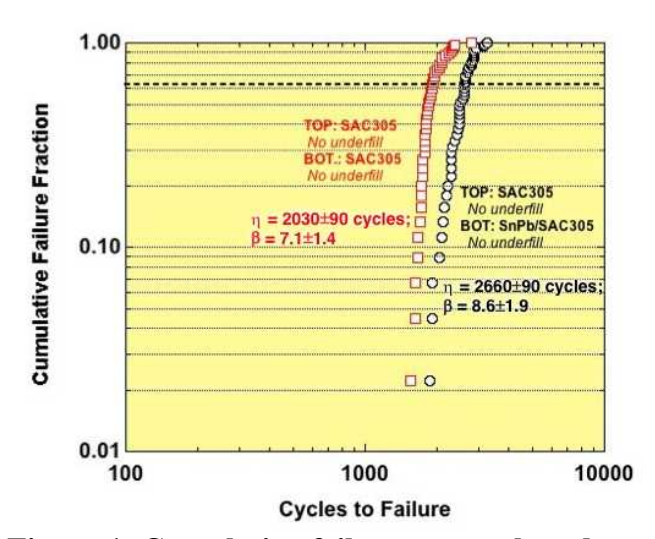


Figure 1. Cumulative failures were plotted as a function of cycles to failure. Both test vehicle types had 100% SAC305 solder joint on top ("TOP: SAC305"). One variant had 100% SAC305, bottom joints ("BOT: SAC305") and the other had the backward compatible bottom interconnections ("BOT: SnPb/SAC305"). The mean values and $\pm 95\%$ confidence interval error terms are provided for η and β on the plots. The dashed line designates the 0.63 fraction (or 63% failed) [4].

A second factor, which is of particular importance to high-reliability military and space electronics, is the use of underfill materials between packages. Underfills provide added assurance that the assembly will survive shock and vibration environments. The previous PoP study demonstrated that the introduction of underfill can negatively impact the reliability of second-level interconnections under temperature cycling

This point is illustrated in Fig. 2, conditions. which shows the cumulative failures for backwards interconnections compatible, bottom (BOT: SnPb/SAC305) without underfill (black squares) as well as with underfill in only the bottom gap (blue circles) or underfill in both gaps (red The introduction of underfill triangles). significantly reduced the characteristic lifetimes (n) of the joints. More so, underfill decreased the "slope" parameter (B), which implies that the probability distribution of failure was widened by the presence of underfill, thereby increasing the uncertainty when predicting N_f.

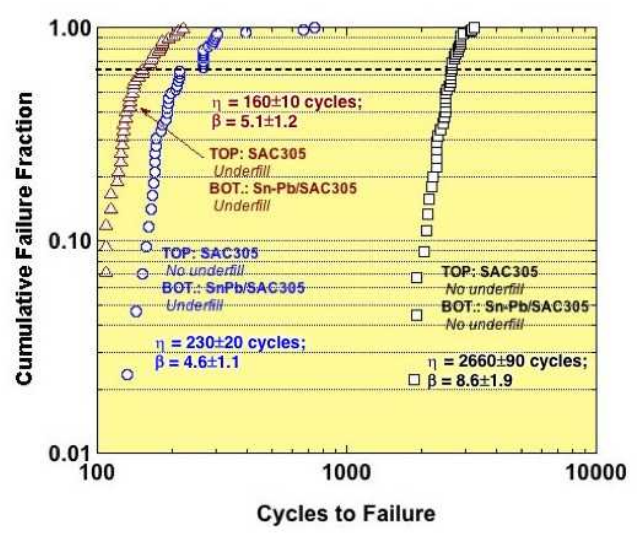


Figure 2. Cumulative failures were plotted as a function of cycles to failure. All test vehicles had 100% SAC305 solder joint on top ("TOP: SAC305") and backwards compatible, bottom interconnections ("BOT: SnPb/SAC305"). The black squares describe the N_f values when there is no underfill; blue circles represent assemblies having underfill only in the bottom gap; and red triangles are for the test vehicle with underfill in both gaps. The dashed line designates the 0.63 fraction (or 63% failed) [4].

A similar analysis was performed on PoP assemblies having 100% Pb-free solder joints. Figure 3 compares the three cases based on underfill use. While the introduction of underfill into one or both gaps caused β to decrease, the η parameter had a mixed trend. Not only was the magnitude of underfill's effect reduced, it also differed when compared to the SnPb/SAC305

interconnections (Fig. 2). These results clearly demonstrate the complex, TMF response of the second-level (bottom) solder joints to their alloy composition as well as to the absence or presence of underfill.

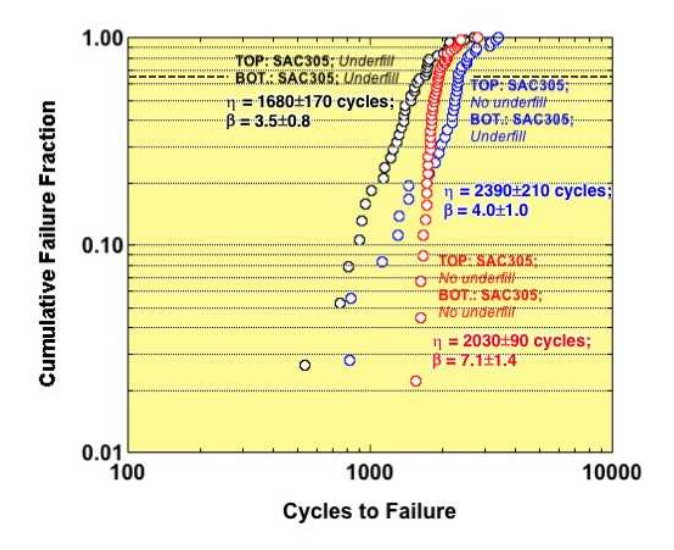


Figure 3. Cumulative failures were plotted as a function of cycles to failure. All test vehicle had 100% SAC305 solder joints for the top and bottom interconnections. The red circles describe the N_f values when there is no underfill in either gap. Blue circles represent assemblies having underfill only in the bottom gap. Black circles refer to test vehicles with underfill in both gaps. The dashed line designates the 0.63 fraction (or 63% failed) [4].

The data analysis associated with reference 4 included a study of the relationship between cycles to failure versus the temperature at which N_f took place. This analysis is exemplified by the findings shown in Fig. 4, which were obtained from the test vehicles having 100% SAC305 bottom solder joints. The three symbol colors represent the three underfill conditions as noted in the legend. In the case of no underfill, whatsoever, the failures are distributed, more-or-less uniformly, across the temperature range. On the other hand, when underfill was present in the bottom gap or in both failures occurred preferentially gaps, temperatures above 25°C. This trend indicated that the thermal expansion of the underfill and, in particular, that in the bottom gap, caused a vertical load between the PoP and PCB that contributed to solder joint TMF performance. The consequence

was not so much, a dramatic decrease of characteristic life (η), but more so, a widened the failure distribution indicated by a decrease of β .

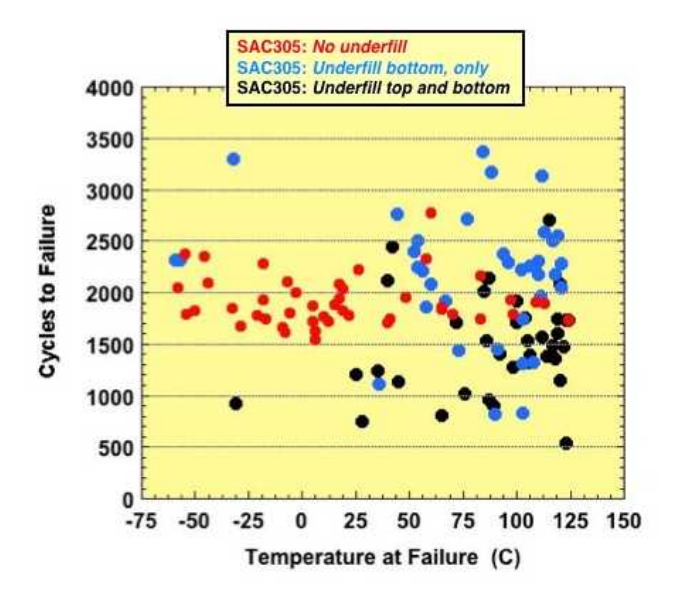


Figure 4. Cycles to failure (N_f) were plotted as a function of temperature at failure. All test vehicle had 100% SAC305 solder joints for the top and bottom interconnections. The circle color pertains to the presence of underfill in the gaps [4].

The studies described above empirical demonstrated the non-intuitive nature of the TMF response of the solder interconnections. source of these trends was the inherent complexity of the PoP structure, which was made more so by of underfill addition Under circumstances, computational modeling becomes an attractive tool with which to "sort out" the primary and secondary contributing factors to solder joint reliability performance. The modeling effort, which was described in reference 5, had sufficient fidelity to predict relative TMF performance between different PoP configurations. However, the capability to predict absolute N_f values, which would allow the model to serve as a product design tool, required an improved database of material properties for the PoP structural members, underfill, and the PCB.

The present report describes the results of the second phase of the stacked packaging project at Sandia. This effort addressed the TMF

performance of PoPoP interconnections. The same methodology was followed in this work. First, failure rate data were collected from thermal cycling experiments using daisy chain test vehicles and the event detection methodology based on the IPC-9701A specification. Failure analysis was critical for correlating the N_f data to the microstructure of the solder joints. Follow-up development efforts addressed the of computational modeling tool predict interconnection TMF. The objective is to validate those predictions with the empirical data on the path towards developing a design tool.

EXPERIMENTAL PROCEDURES Area-array components

Commercially-available, daisy chain PoPoP components and PCBs were assembled into PWA test vehicles. The PCB was constructed of a 1mm thick, high-temperature ($T_g = 180^{\circ}C$) FR-4 laminate. The Cu pads were coated with an organic solderability preservative (OSP). All fifteen (15) component sites were populated with a PoPoP package. The schematic diagram in Fig. 5 shows the PoPoP configuration. The solder joints between the top and middle packages, as well as those between the middle and bottom packages, are considered to be first-level interconnections although they are made during the assembly process that also formed the second-level interconnections between the bottom package and the PCB.

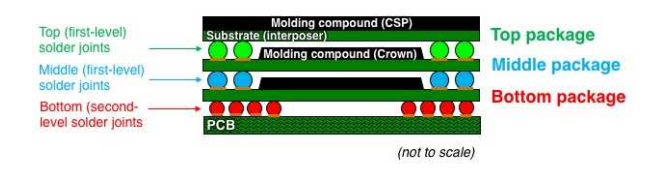


Figure 5. Schematic diagram shows the construction of the PoPoP component as well as the *package* and *solder joint* nomenclatures.

The details of the package configurations are listed, below:

• **Top package:** molding compound is in a chip-scale package format having a 12 x 12 mm footprint; substrate finish, electroless Ni, immersion Au (ENIG); 128 I/O; and

0.65 mm pitch, two-row perimeter array of 96.5Sn-3.0Ag-0.5Cu (SAC 305) solder balls.

- Middle package: molding compound is in a crown configuration having a substrate footprint of 12 x 12 mm. *Top*: two-row perimeter array of 128 I/O pads, 0.65 mm pitch, ENIG finish. *Bottom*: 128 I/O of 98.5Sn-1.0Ag-0.5Cu (SAC 105) solder balls on the same 0.65 mm pitch; and ENIG finish.
- **Bottom package:** molding compound is in a crown configuration having a substrate footprint of 12 x 12 mm. *Top*: two-row perimeter array of 128 I/O pads, 0.65 mm pitch, and ENIG finish. *Bottom*: 305 I/O of SAC305 solder balls on a 0.50 mm pitch; and bare Cu.

Test vehicle assembly

A two-step sequence was used to assemble the test vehicles. The need for a two-step method rather than the more efficient single pass process, was warranted by the backwards compatibility test vehicles. In those latter variants, the decision was made to use a lower temperature SnPb process profile in order to increase the likelihood that the second-level (bottom) interconnections would be a worst-case, that is, poor mixing of the SnPb paste and SAC305 solder ball. Prior studies have suggested that there is reduced TMF reliability by a non-homogeneous microstructure that results from poor alloy mixing. However, there was the possibility that the low-temperature SnPb reflow would not melt the above SAC305 and SAC105, first-level interconnections. Therefore, a prior step, termed the "stack reflow," was performed using a higher peak temperature so as to optimize the quality of the top and middle (first-level) interconnections. In order to assure that the top and middle solder joints were consistent across all of the test vehicles, the same two-step process was also used to assemble the 100% SAC305 secondlevel (bottom) interconnections, as well.

The two-step process is shown schematically in Fig. 6. A tacky flux is applied to the solder balls of the top and middle packages. Those two packages

are assembled on top of one another and then, placed atop the bottom package. The three

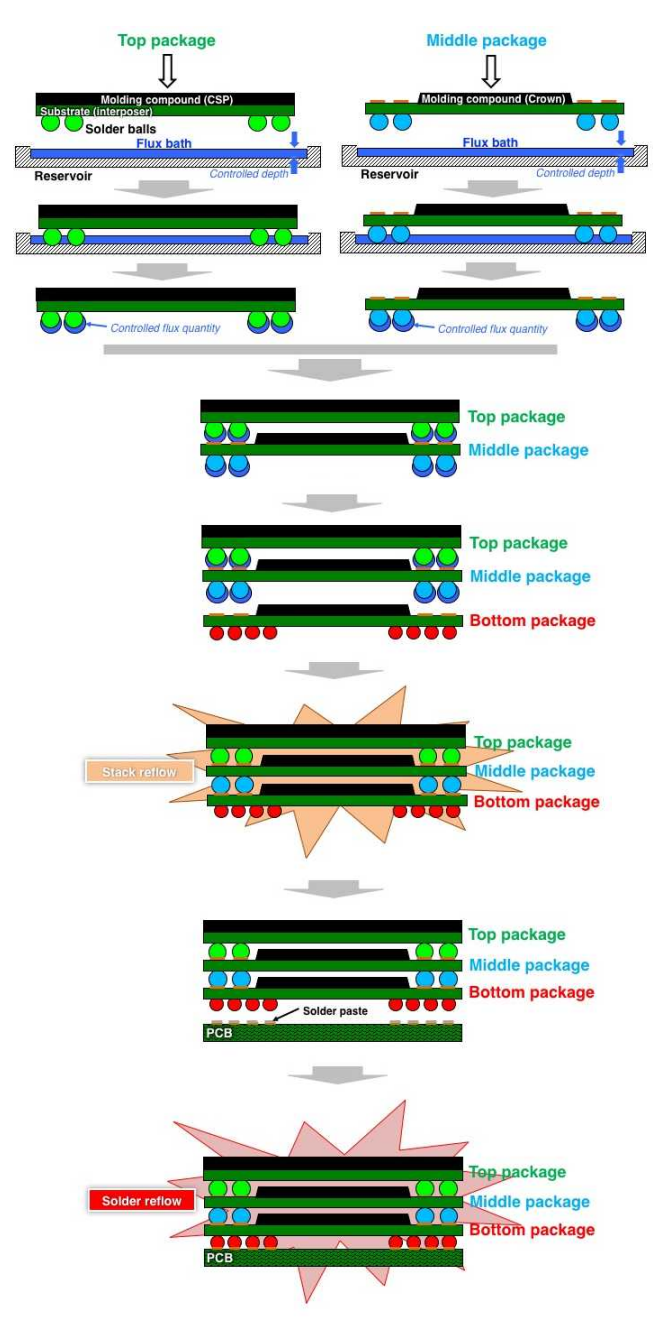


Figure 6. Schematic diagram shows the two-step assembly sequence. First, the individual packages are assembled by the stack reflow to complete the PoPoP component. Then, the PoPoP component is assembled to the PCB using the solder reflow step to complete the PWA test vehicles.

packages are placed through the "stack reflow" step that forms the two layers of first-level interconnections that complete the PoPoP

component. Next, the SnPb or SAC305 solder paste is printed on the PCB Cu pads. The PoPoP is picked up and placed on the PCB so that the solder balls rest on the paste. The assembly was then passed through the solder reflow oven to form the second-level, bottom interconnections. As noted above, low temperature and high temperature process profiles were utilized for the mixed SnPb/SAC305 and SAC305 pastes, respectively. A total of twenty (20) test vehicles were assembled with each of the SnPb paste (backwards compatibility) and SAC305 paste (100% Pb-free). A photograph is shown in Fig. 7 of the test vehicle.

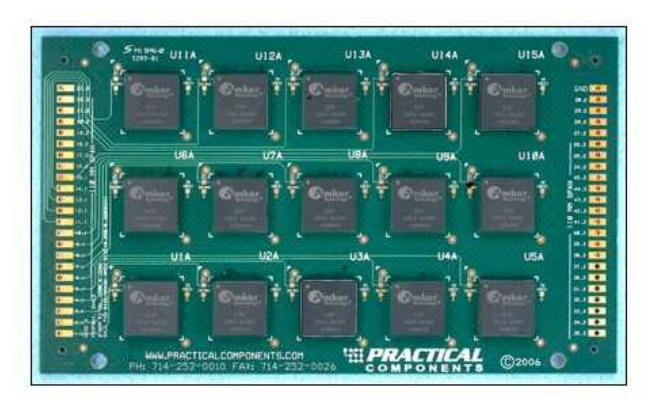


Figure 7. Photograph of the PoPoP test vehicle

Underfill

Sub-sets of test vehicles were created from each of the two second-level assembly types – 100%SAC305 versus mixed SnPb/SAC305 – for the underfill test matrix. The four configurations of underfill and the number of test vehicles made per each configuration are listed below:

- No underfill, N=8
- Bottom gap, only, N=4
- Bottom and middle gaps, N=4
- Bottom, middle, and top gaps, N=4

The underfill was a thermal setting material with a glass transition temperature (T_g) = 120°C, which is just below the maximum temperature of 125°C in the thermal cycle. At temperatures less than T_g , the (x, y) and (z) coefficients of thermal expansion (CTE) had values of 22 – 23 ppm/°C. Above T_g , the values climbed to 83 – 85 ppm/°C. Since the glass transition is actually a relatively gradual change of mechanical and physical properties, the

high temperature end of the thermal cycle (approximately $100 - 125^{\circ}\text{C}$) will likely overlap the glass transition and the effects of changing materials properties. The underfill was applied after the final assembly step and was cured by a 30 min exposure to 150°C. The photograph in Fig. 8 shows a PoPoP package having underfill in the middle and bottom gaps, but not in the top gap where the solder balls are clearly visible.

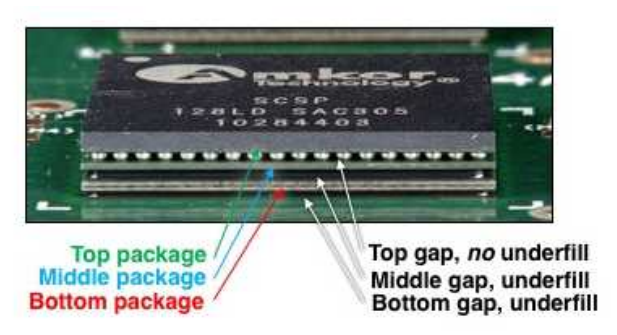


Figure 8. Photograph shows the PoPoP having underfill in the middle and bottom gaps, but not in the top gap.

Thermal cycling

The accelerated aging test was based upon thermal cycling. The parameters are listed here:

• Minimum temperature: -55°C

• Maximum temperature: 125°C

• Hold times at the temperature limits: 15

• Ramp rates: 10°C/min

• End of testing: 10,000 cycles.

Quantitative failure data were collected according to the procedures in IPC-9701A. An additional requirement, which was set-forth in the Sandia program, was that the loop remain in the open condition through TWO, 50 cycle intervals before being "officially" declared as a failure. There was only one circumstance in which the loop failed once, but did not fail immediately upon continuation of the cycles. A photograph is provided at the top of Fig. 9, which shows the test vehicles and stacking within the thermal cycling chamber. The schematic diagram at the figure bottom illustrates the solder joint nomenclature.



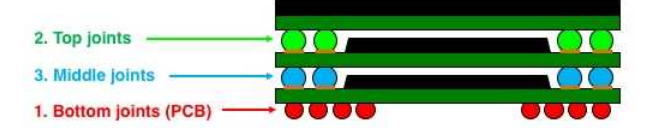


Figure 9. At the top of the figure is a photograph that shows the test vehicles and wiring that connects them to the event detector (outside the chamber). The nomenclature used to designate the three solder joint layers is shown at the bottom of the figure: top joint (2); middle joints (3); and bottom joints (1).

The PoPoP test vehicles were used in the following manner: Duplicate copies were selected per each second-level interconnection type, i.e., 100% (backwards SAC305 versus SnPb/SAC305 compatible) and for each of the aforementioned underfill conditions. These test vehicles were wired-up to the event detector to capture two of three interconnection layers. The interconnection layer nomenclature is illustrated at the bottom of Fig. 9: top joint (2); middle joints (3); and bottom joints (1). The first of the two test vehicles is used to monitor the bottom (1) and middle (3) solder joints while the second PWA monitors the bottom (1) and top (2) solder joints. The point is raised that the signals from the top (2) and middle (3) solder joint layers must pass through bottom solder The latter interconnections were ioints (1). selected to have the least likelihood to fail in order to capture, explicitly, the reliability of the middle and top interconnections.

Unfortunately, a competition of sorts arises between the acquisition of quantitative (event detection) failure data versus the microanalysis required to establish the failure mode. As noted above, the signals for the middle (3) and top (2)

solder joints pass through the bottom (1) interconnections. By-and-large, the bottom solder joints were the first to fail amongst most (not all) of the PoPoP assemblies. In an effort to capture the crack behavior in those bottom interconnections, they were removed from the test vehicle immediately after failure to prevent unwanted damage to their microstructure caused by additional cycles. However, their removal resulted in failure data being no longer collected from the middle and top solder joint. It was later determined that in such cases, the middle and top solder joints actually had significantly longer TMF lifetimes, in some cases, well beyond the 10,000 cycle limit.

In the interest of keeping this report to a reasonable length, only the failure data and microanalysis results will be presented that were obtained from the following cases:

- No underfill,
- Bottom gap, only,

Both bottom solder joint compositions, backward compatibility SnPb/SAC305 and 100% SAC305, are included in the discussion. The failure data of the remaining configurations will be compiled and placed in a follow-up report.

Data analysis

The failure data obtained from the event detector output were analyzed by fitting them to the two-parameter (2P) Weibull failure probability distribution function (CDF). The mathematical expression is shown below:

$$CDF(N) = 1 - \exp[-(N/\eta)^{\beta}]$$
 (1)

where N is the number of cycles to failure; η is the characteristic life; and β is the slope.

The error terms for η and β were the respective 95% confidence intervals. All analyses were performed using a commercial statistical software.

A second analysis was made whereby the temperature at which the joint failed (per the above criterion) was plotted as a function of $N_{\rm f}$. The premise of this approach is that, when TMF is due

primarily to shear deformation and the solder joints are not impacted by other stress contributions, a random distribution should characterize the failure temperatures. On the other hand, when tensile/compression stresses caused by z-axis thermal expansion contribute significantly to TMF, failure is more likely to occur at elevated temperatures.

If there are residual stresses remaining in the solder, e.g., due to cool down from solidification or curing of the underfill, then further cooling should increase those stresses. As a result, failures would be more prevalent when the stress grows from 25°C to -55°C, which would appear with the failure temperatures showing a preference for the lower range of values.

Unfortunately, tension and compression stresses due to warpage effects cause the failure analysis to become more complicated for the failure temperature data. The complexity arises from synergistic effects between the individual package structures; the underfill placement; and the PCB structure.

Microanalysis – cross sections

Individual packages were routed out of the PCB using a technique that avoided severing the connections of, or otherwise causing damage to, the neighboring packages. The equipment and example of a routed PWA are shown in Fig. 10.

After being routed out of the PCB, the PoPoP component was cross sectioned according to the map in Fig. 11. Three sections were made: section 1, full diagonal; section 2, one-half diagonal; and section 3, perimeter row. The macro views of the solder joints are shown for sections 1 and 3.

The point is made here that the failure analysis portion of this study could quickly overwhelm the other tasks. It was not possible to assess three cross sections from thirty PoPoP components (duplicate test vehicles having fifteen components per test vehicle). Therefore, it was necessary to analyze the physical metallurgy of the interconnections from a limited number of strategically selected PoPoP components.

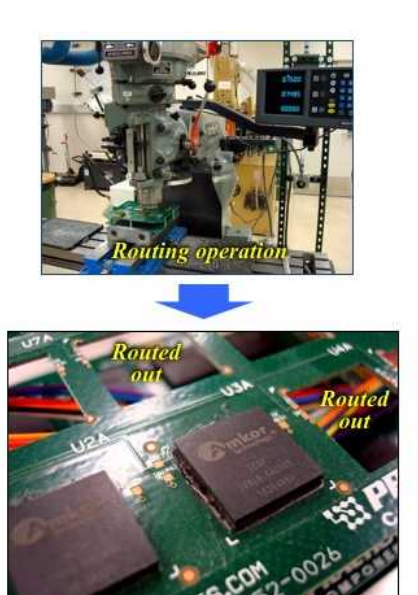


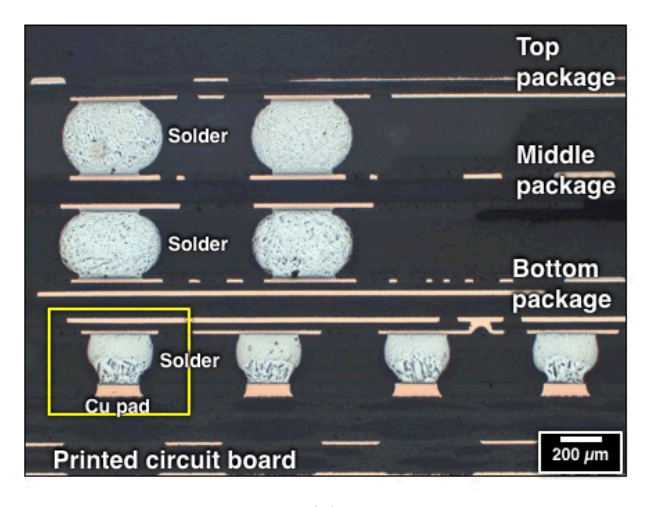
Figure 10. Photographs show the routing operation and the PWA after several of the PoPoP components had been routed out of it.



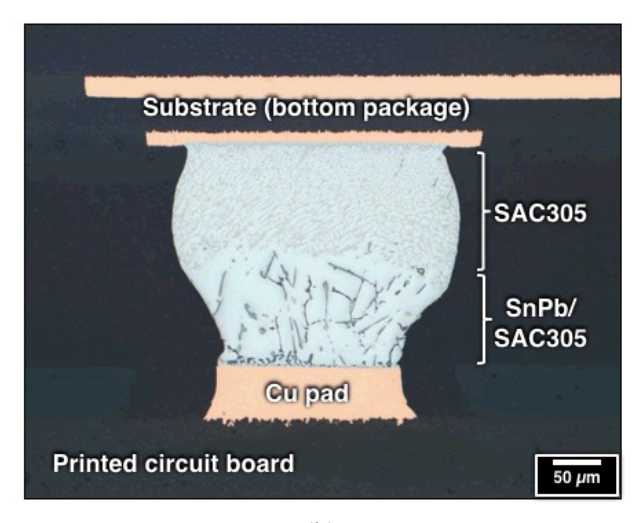
Figure 11. Schematic diagram identifies the locations of the three cross sections made to the PoPoP component. Micrographs show the views of the solder joints in sections 1 (full diagonal) and 3 (perimeter).

RESULTS AND DISCUSSION As-fabricated solder joint microstructure

Recall that an objective of the assembly process designed for the backwards compatibility test vehicles (mixed SnPb/SAC305) was to generate a non-homogeneous microstructure. Towards that goal, the process was successful for *only one* PWA, S/N05. Figure 12a shows the stack of solder joints



(a)



(b)

Figure 12. (a) Photograph shows one-half of the cross section 1 showing the three levels of solder joints on of U01 on test vehicle S/N05 (asfabricated condition with underfill in the middle and bottom gaps). The bottom solder joints show the non-homogeneous microstructure of backwards compatibility. (b) High magnification image shows the solder joint in the yellow box of (a). The mixed SnPb/SAC305 segment is at the bottom of the joint and the remaining SAC305 microstructure of the original solder ball is identified at top.

between the three packages from one side of section 1 of the U01 component (representing the as-fabricated condition and underfill in the bottom and middle gaps). These bottom interconnections and, in fact, all of them observed throughout sections 2 and 3 of U01, developed the same non-homogeneous microstructure. The micrograph in

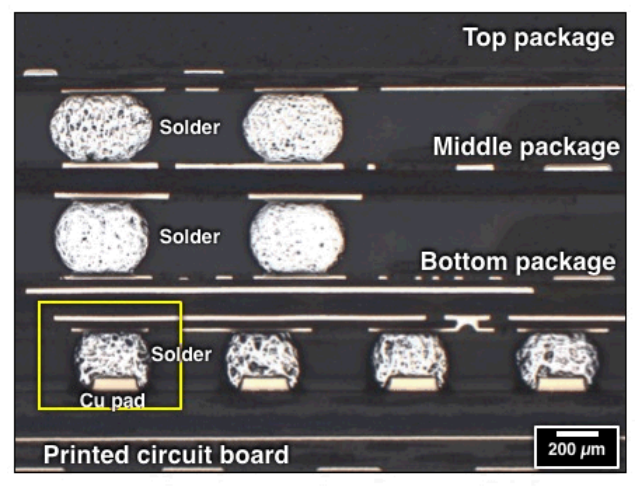
Fig 12b is a high magnification image of the bottom interconnection identified by the yellow box in Fig. 12a. Intermixing occurred at the bottom of the joint while the top portion showed only the SAC305 microstructure. In fact, energy dispersive x-ray (EDX) analysis confirmed that a sharp compositional boundary existed whereby Pb was absent from the upper SAC305 microstructure.

The non-homogeneous microstructure is accompanied by an "hour-glass" profile to the solder joint. The spreading of the intermixed zone upwards varied slightly between the various solder joints as shown in Fig. 12a. In all cases, cracks were not observed in the joints. Void formation did not occur to a greater propensity in the non-homogeneous interconnections than it did in *any* other joints, regardless of composition or level.

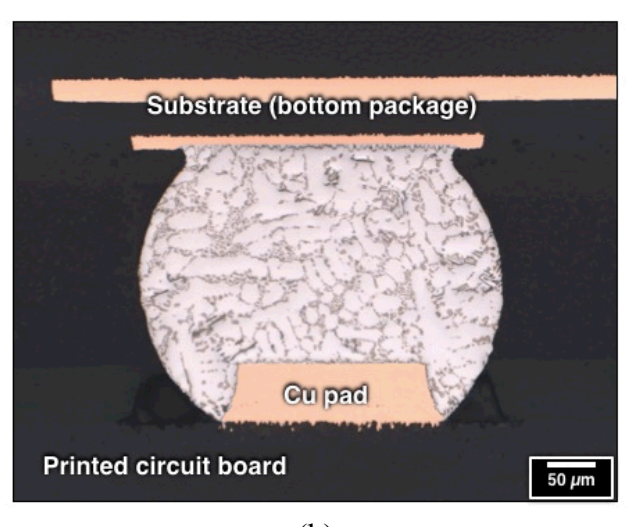
The remainder of the backward compatible PWAs exhibited complete mixing within the bottom interconnections. The low magnification image to Fig. 13a was taken of the test vehicle S/N07 (U01 component, representing the as-fabricated condition and underfill only in the bottom gap). The microstructure was homogeneous across vertical dimension. This characteristic is further illustrated by the high magnification image in Fig. 13b.

The consistent formation of a non-homogeneous microstructure was not achieved for the backwards compatible test vehicles. However, this observation implies that there is a relatively sharp process cutoff between the two microstructural outcomes. Therefore, it should be relatively easy to avoid the non-homogeneous case through nominal process development efforts. Also, the extent of the SnPb/SAC305 zone varied only slightly, joint-to-joint. Therefore, in the event that this microstructure does occur, the solder joints should exhibit a relatively consistent degree of TMF performance across the component.

Unfortunately, the S/N05 test vehicle was not in the group that were connected to the event detector. Therefore, it was not possible to determine, *statistically*, any difference in reliability between



(a)



(b)

Figure 13. (a) Photograph shows one-half of the cross section 1 and the three levels of solder joints on the U01 component of test vehicle S/N07 (representing the as-fabricated condition with underfill in the bottom gap) showing a homogeneous microstructure. (b) High magnification image shows the homogeneous microstructure across the solder joint in the yellow box of (a).

its non-homogeneous interconnections and the homogenous solder joints of the other backward compatible test vehicles. On the other hand, S/N05 and S/N07 test vehicles, as well as six other PWAs representing variants of SnPb/SAC305 versus 100% SAC305 bottom solder joints and underfill applications, "rode along" with the event detected units in the temperature cycling chambers. Components were milled out of these "ride along"

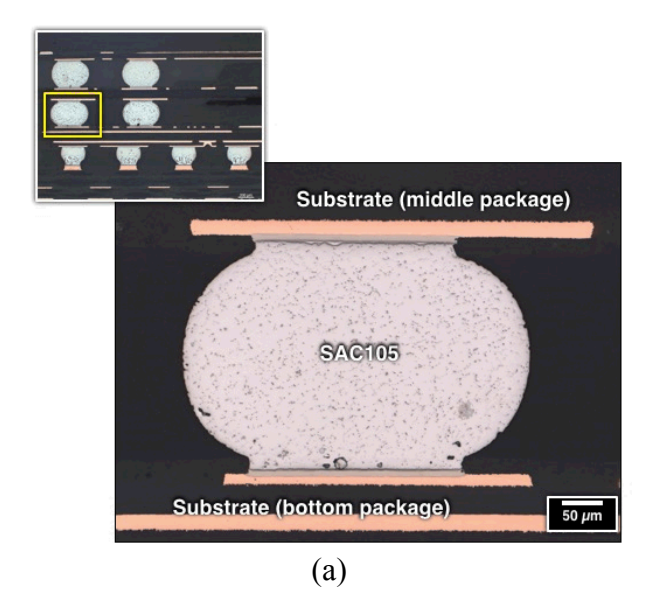
test vehicles (see Fig. 10) at the completion of 600, 1000, 1500, 2500, 5000, and 7000 cycles. The components were cross sectioned (see Fig. 11) to document the extent of TMF deformation in the interconnections. Therefore, a comparison, albeit only qualitative, can be assessed of the extents of **TMF** that occurred between the microstructures representing backwards compatibility in these PoPoP components. In the interest of brevity, these specific results will be described in a follow-on report.

Finally, there was a noticeable degree of warpage to the PoPoP packages upon completion of the second-level assembly process. **Ouantitative** measurements were not made of warpage on the components. However, extensive observations were compiled of packages on all of the test vehicles. The warpage did not cause damage to the dice, molding compound, or substrate structures. Also, there was very limited distortion to the second-level (bottom) solder joints attributable to A past study, which included both warpage. empirical data and computational modeling, confirmed that the vertical distortion interconnections caused by warpage has very limited impact on their TMF performance [6].

Although the focus has been placed on the compatible solder backwards joints, microanalysis also examined the middle (SAC105) and top solder joints (SAC305). The micrographs in Figs. 14a and 14b exemplify the microstructures that were observed for these two interconnections. Aside from slightly greater distortion to the middle SAC105 joints caused by warpage, these and the interconnections exhibited adequate top solderability and the absence of significant void formation or other defects. Therefore, the reduced temperature profile used to reflow the SnPb paste did not have an adverse effect on the first-level interconnections.

The cross section analysis was also directed to those test vehicles having 100% SAC305 bottom solder joints, including the different underfill variants. In all cases, the bottom interconnections exhibited excellent solderability and very minimal void formation (appearing not unlike the joint in

Fig. 14b, except for a different Cu pad on the PCB.) Moreover, the middle and top interconnections similarly showed excellent solderability and an absence of any defects, recalling that they would have been reflowed a *second time* by the solder reflow process (Fig. 6) that assembled the PoPoP component to the PCB.



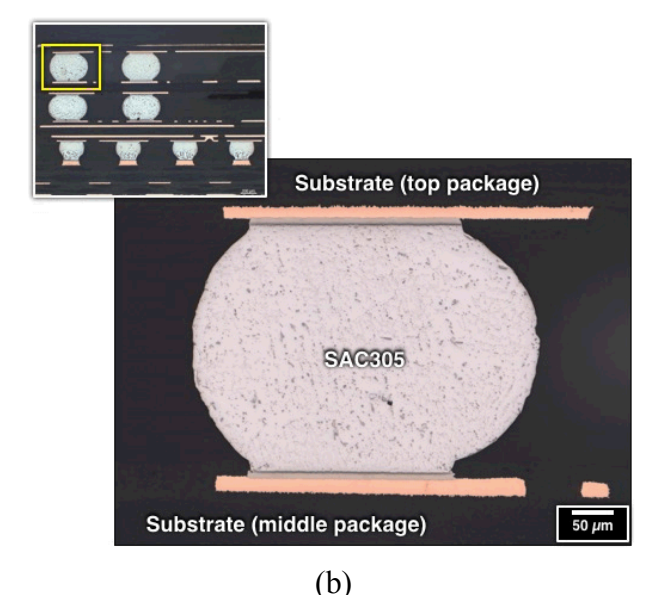


Figure 14. (a) Photograph shows a middle SAC105 solder joint (yellow box of the inset image) taken from the U01 component on the S/N05 test vehicle (representing the asfabricated condition with underfill in the middle and bottom gaps). (b) Similar micrograph shows the top level, SAC305 solder joint.

Post-thermal cycle data

The failure data are presented, below, according to the bottom (second-level) solder joint pedigree – mixed SnPb/SAC305 or 100% SAC305 – and whether or not, underfill was present in the bottom gap. The microstructure failure analysis is included in the discussions.

Mixed SnPb/SAC305 bottom interconnections; no underfill.

The log-log plot is shown in Fig. 15 of cumulative failure fraction as a function of cycles to failure, $N_{\rm f}$. These results reflect the combination of data obtained from test vehicles S/N22 and S/N23. The data were color-coded to represent the bottom, middle, and top solder joints. All of the data showed a very similar failure behavior. This finding is interesting, not only from the fact that all these solder joint have different compositions, but also from the aspect that the reliability of the PoPoP as a whole, can potentially be represented by a single probability distribution.

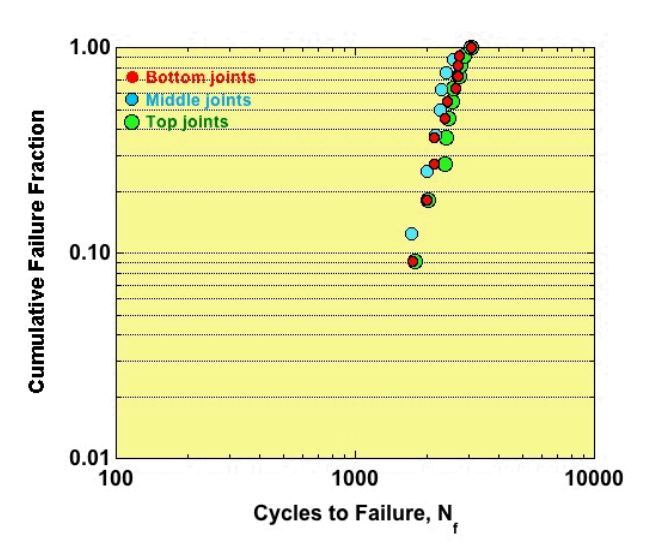


Figure 15. Log-log plot shows cumulative failure fraction as a function of cycles to failure for each of the three levels of solder joints: bottom; middle; and top. The data were obtained from S/N22 and S/N23 test vehicles that represent the mixed SnPb/SAC305 bottom interconnections and an absence of underfill from any of the gaps.

The similarity of TMF failure behaviors was confirmed, quantitatively, when the 2P Weibull analysis was applied to the failure data. The

characteristic lifetime (η) and slope (β) parameters are listed below for each solder joint level:

Top solder joints:

 $\eta = 2600\pm200 \text{ cycles}; \beta = 8.7\pm4.0$

Middle solder joints:

 $\eta = 2500 \pm 300 \text{ cycles}; \beta = 6.6 \pm 3.4$

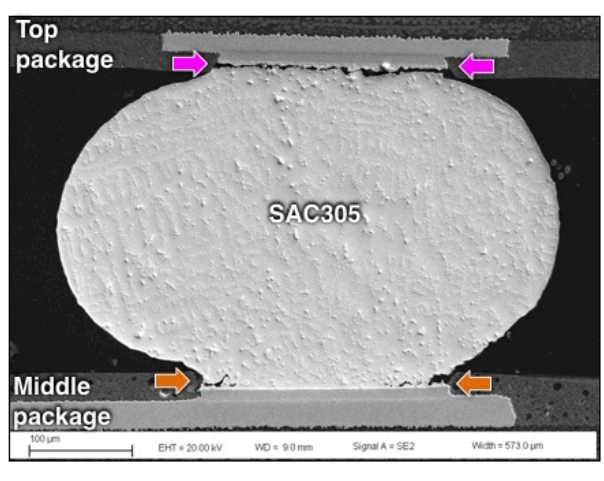
Bottom solder joints:

 $\eta = 2600\pm200 \text{ cycles}; \beta = 7.6\pm3.5$

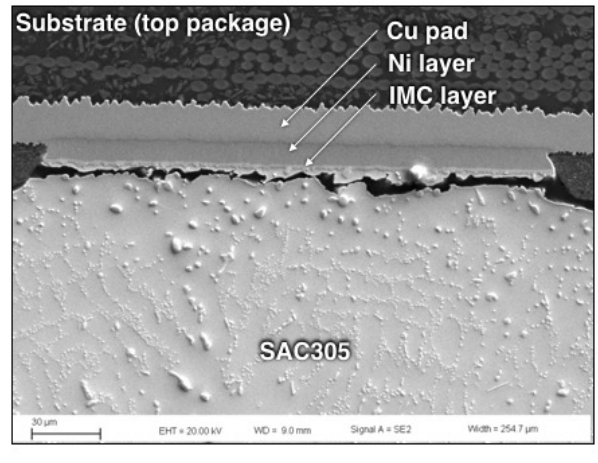
The limited number of data points per solder joint type caused the increase error terms. The characteristic lifetimes (η) were the same between all three cases to within experimental error. Slightly greater variations were observed in the slope parameters (β), although they did not differ, statistically, according to the 95% confidence intervals. In addition to the geometric differences between the top and middle interconnections, the different alloy compositions (SAC305, top; and SAC105, middle) can be a contributing factor to the slightly different, mean β values between them.

The similarity of failure rates between *all* three solder levels was further substantiated by crack development in the solder joints. A top solder joint is shown by the SEM photograph in Fig. 16a, which originated from the component U10A of S/N22. That loop failed at 3068 cycles. A 100% TMF crack can be observed at the top side (magenta arrows) and partial cracks at the bottom side (orange arrows) of the joint profile. The high magnification image in Fig. 16b shows that the top crack, which would have certainly caused an electrical open, exhibited the growth behavior typical of TMF, that is, in the solder near to the solder/pad (Ni finish) interface.

The event data indicates that the middle solder joints experienced a similar failure rate as the top level interconnections. However, the crack preferred to propagate at the bottom of the joint. This point is illustrated by the SEM image in Fig. 17a. Often, the crack path is somewhat circuitous within the SAC305 microstructure, but remains close to the pad.



(a)



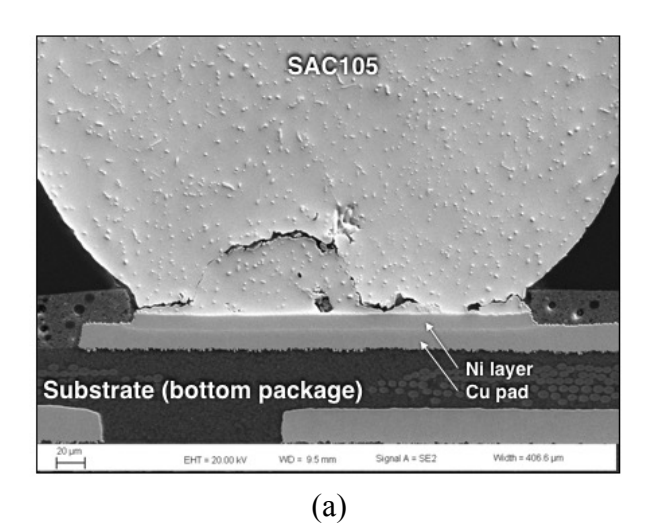
(b)

Figure 16. (a) SEM image shows a solder joint on the top level of S/N22, package U10A (no underfill). The associated daisy chain failed at 3068 cycles. (b) High magnification SEM image shows the 100% crack at the top of the joint.

The bottom interconnections experienced TMF cracking at the top of the joint as shown by the magenta arrow in the SEM image that is Fig. 17b. The available cross section did not capture a 100% crack condition. The backscattered electron (BSE) image was preferred for Fig. 17b in order to illustrate the homogeneous distribution of Pb-rich phase (light gray tone) in the mixed SnPb/SAC305 microstructure. A definitive conclusion could not be established that the defect above the PCB Cu pad was, or was not, a crack.

Given the similar failure statistics between the three solder joint levels, the data were combined together to represent the S/N22 and S/N23 test vehicles (SnPb/SAC305 bottom interconnections and the absence of underfill). The cumulative failure fraction plot is shown in Fig. 18. The 2P Weibull parameters are listed below:

Combined (top, middle, and bottom) solder joints: $\eta = 2600\pm100$ cycles; $\beta = 7.5\pm2.1$



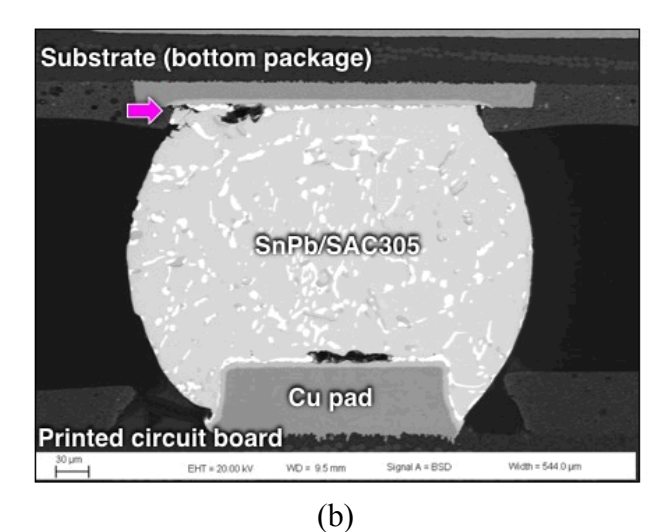


Figure 17. (a) SEM image shows a solder joint on the middle level of S/N22, package U10A (no underfill) that is 100% cracked. The associated daisy chain failed at greater than 3068 cycles. (b) High magnification SEM, backscattered electron (BSE) image shows crack position near the top of a bottom solder joint.

The larger sample count clearly reduced the 95% confidence intervals of both η and β . Both S/N22 and 23 performed similarly. Lastly, there were no

outliers in the graph. Typically, outliers occur towards the *lower* cycle counts because they originate from infant mortality failures.

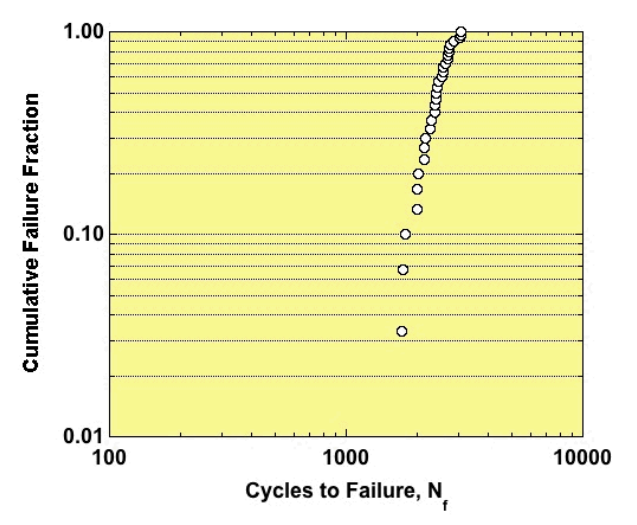


Figure 18. Log-log plot shows cumulative failure fraction as a function of cycles to failure that combines data from all three levels of solder joints from the S/N22 and S/N23 test vehicles. The bottom interconnections had the mixed SnPb/SAC305 composition and underfill was not present in the gap.

The plot of failure temperature as a function of $N_{\rm f}$ is shown in Fig. 19. The data are combined from

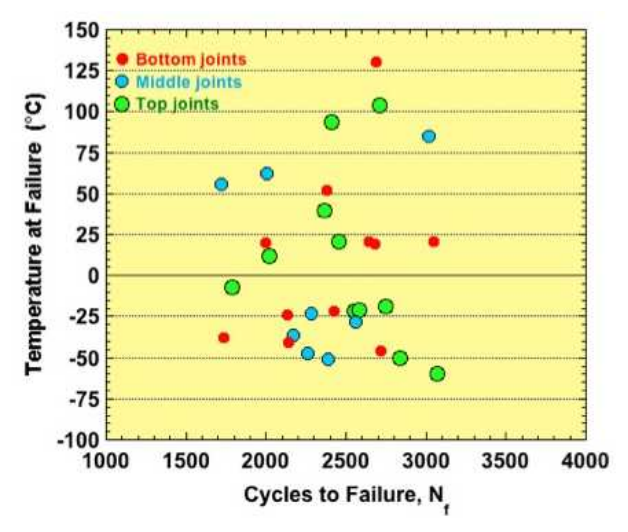


Figure 19. Temperature at failure was plotted as a function of cycles to failure (N_f) for the S/N22 and S/N23 test vehicles that represent the mixed SnPb/SAC305 bottom interconnections and an absence of underfill from the gap. The symbol colors indicate the solder joint locations.

both S/N22 and S/N23 and color coded according to the location of the solder joints. At first glance, the temperature at failure appears to be relatively distributed across the entire span of temperatures. However, if the assumption is made that the solder joints are "stress-free" at 25°C owing to creep relaxation, then it appears that failures occurred with a slight preference for colder temperatures. The loss of compliance at the low temperatures impose higher stresses on the solder joints that increase the probability of failure. Nevertheless, the shear deformation largely controlled TMF as evidenced by the crack morphologies in Figs. 16 and 17.

100% SAC305 bottom interconnections; no underfill.

The failure data are examined, which were obtained from the test vehicles S/N44 and S/N45. The PoPoP components had 100% SAC305 bottom (second-level) solder joints. The log-log graph of cumulative failure fraction versus cycles to failure is shown in Fig. 20. When compared to Fig. 15,

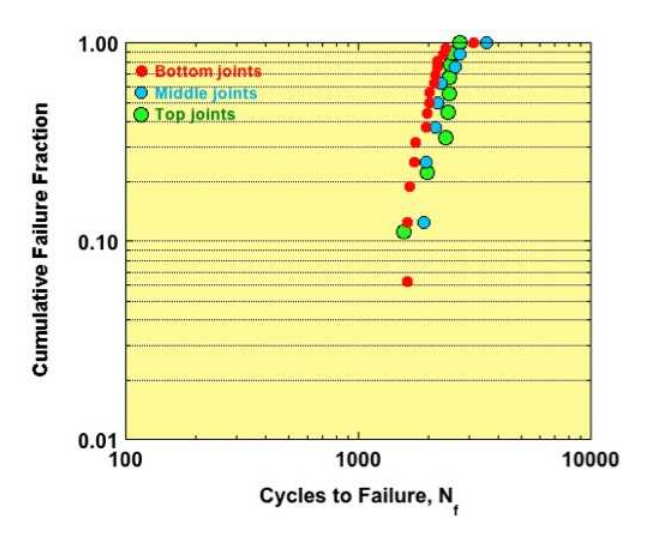


Figure 20. Log-log plot shows cumulative failure fraction as a function of cycles to failure for each of the three levels of solder joints: bottom (second-level); middle; and top. The data were obtained from S/N44 and S/N45 test vehicles that represent the 100% SAC305 bottom interconnections and an absence of underfill from any of the gaps

there was a slight difference between the three interconnection levels. Therefore, the analysis began by preforming the statistical analysis on the individual solder joint levels.

The 2P Weibull parameters are listed below for each of the three interconnection genres:

Top solder joints:

 $\eta = 2400\pm200 \text{ cycles}; \beta = 10.6\pm6.0$

Middle solder joints:

 $\eta = 2600\pm500 \text{ cycles}; \beta = 5.0\pm2.0$

Bottom solder joints:

 $\eta = 2200\pm200 \text{ cycles}; \beta = 5.2\pm2.0$

The mean values of characteristic lifetime (η) differed slightly between the three layers, but were considered to be, statistically similar. The slope (β) value of the top solder joints (SAC305) was high, indicating a relatively tight distribution of failures. The middle interconnections (SAC105) had a lower β value as did also the bottom solder joints (100% SAC305).

Typically, lower-than-expected β values are caused by low N_f outliers arising from infant mortality failures. However, when the middle and bottom solder joint data sets were re-evaluated, it was observed that high N_f outliers were responsible for the low β values. Neither of the two high N_f instances exhibited unusual behaviors to warrant that they be removed from the respective analysis. Nevertheless, the Weibull analyses were re-executed on the middle and bottom solder joint data after removal of those outliers. The results are shown below:

Middle solder joints:

 $\eta = 2400\pm300 \text{ cycles}; \beta = 8.2\pm4.7$

Bottom solder joints:

 $\eta = 2100\pm100 \text{ cycles}; \beta = 9.6\pm3.8$

There was a small reduction in the η values as expected by the loss of the high outliers. However, the slope value nearly doubled, indicating a

significant tightening of the failure distribution. The 95% confidence terms also increased with a reduction of β because the increased slope also amplifies the error term.

The failure data were combined together that were obtained from the three solder joint levels of both test vehicles. The 2P Weibull parameters are listed below:

Combined (top, middle, and bottom) solder joints: $\eta = 2400\pm200$ cycles; $\beta = 5.0\pm1.2$

Next, the combined S/N 44 and S/N45 data were plotted with the combined data from S/Ns 22 and 23, which represent the SnPb/SAC305 backwards compatibility case. This analysis assesses the overall, PoPoP performance between the two conditions of bottom solder joints. The cumulative failure fraction plot is shown in Fig. 21. In the

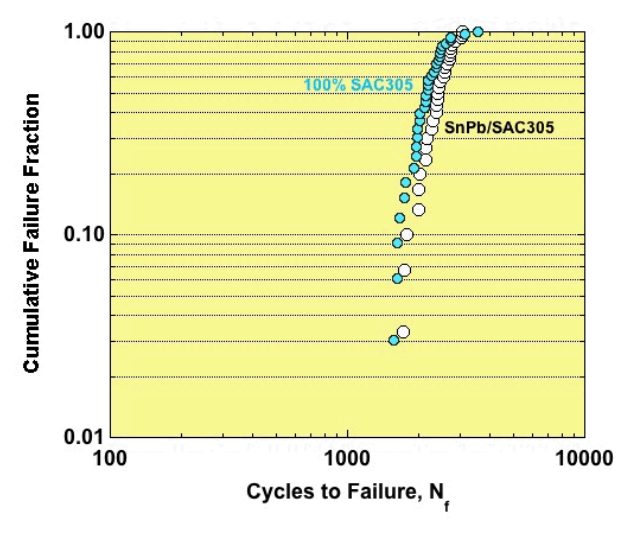


Figure 21. Log-log plot compares the cumulative failure fraction as a function of cycles to failure of 100% SAC305 bottom interconnections (three levels of solder joints combined from the S/N44 and S/N45) versus the backwards compatible solder joints (S/N 22 and S/N23 test vehicles). Both variants did not have underfill in any of the gaps.

absence of underfill, the PoPoP component exhibits only a slightly longer characteristic lifetime with backwards compatible, second-level interconnections than with 100% Pb-free solder joints. But, the differences are within the statistical error of the analysis.

A comparison was also made between 2P Weibull parameters of the individual solder joint levels for the 100% SAC305 test vehicles (S/N44 and S/N45) versus the mixed SnPb/SAC305 test vehicles (S/N22 and S/N23). Those data have been compiled in Table 1. First, attention was given to the top and middle solder joints. In the absence of the underfill, there is a reduced likelihood that the TMF behavior of the bottom joints would couple into, or otherwise affect, the similar performances of the top and middle interconnections. The data in Table 1 confirmed that premise as there was little statistically significant difference between their mean η and β values.

Table 1 2P Weibull Parameters of the SnPb/SAC305 and 100% SAC305 Test Vehicles – *No Underfill*

	SnPb / SAC305		100% SAC305	
	η	β	η	β
Top solder joints	2600	8.7	2400	10.6
	<u>+</u> 200	± 4.0	<u>+</u> 200	± 6.0
Middle solder joints	2500	6.6	2600	5.0
	<u>+</u> 300	± 3.4	<u>+</u> 500	± 2.0
Bottom solder joints	2600	7.6	2200	5.2
	± 200	± 3.5	<u>+</u> 200	± 2.0

The observation was also made that in the case of both test vehicle categories, the top, SAC305, joints exhibited mean η values that were similar to those of the SAC105 interconnections. On the other hand, the middle SAC105 solder joints had a consistently lower, mean β value to within the confidence intervals. This trend could be attributed to the middle location of the SAC105 interconnections; however, the different solder compositions and, as such differences of microstructures, cannot be ruled out as a contributing factor.

A similar evaluation was applied to the bottom solder joints. The SnPb/SAC305 solder joints (homogeneous microstructure as exemplified by Fig. 17b) showed a statistically longer characteristic lifetime than did the 100% SAC305 interconnections. The *mean* slope parameter implied that the mixed solder joints benefited from

a tighter failure distribution than did the 100% SAC305 interconnections, although the respective β values were the same to within statistical error.

In summary, the test vehicles having backwards compatible, SnPb/SAC305 bottom solder joints exhibited an improved TMF performance when compared to the 100% SAC305 interconnections. The middle and top solder joints (SAC305 and SAC105, respectively) exhibited similar characteristic lifetimes. The bottom solder joints controlled the TMF reliability of the PoPoP components as a whole, but not by a significant margin over the middle and top interconnections.

Lastly, the temperatures at failure were examined as a function of N_f. Those data are presented in Fig. 22. The bottom solder joints exhibited failure

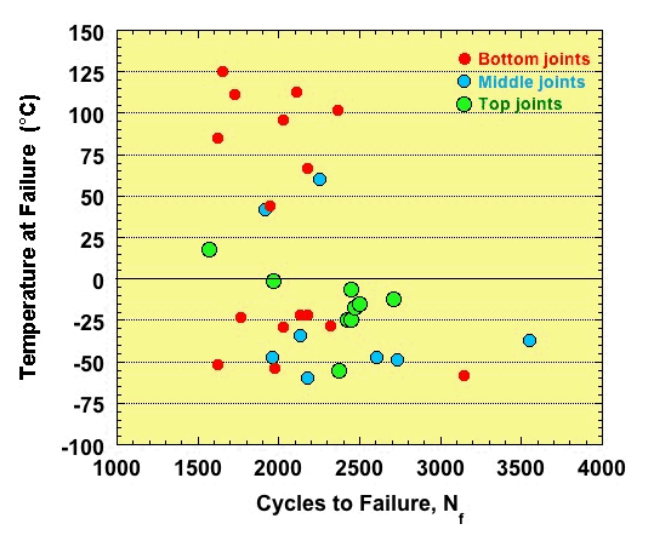


Figure 22. Temperature at failure was plotted as a function of cycles to failure (N_f) for the S/N44 and S/N45 test vehicles that represent the 100% SAC305 bottom interconnections and an absence of underfill from any of the gaps.

temperatures at both the low and high temperature regimes of the thermal cycle. This behavior is slightly different from the case of the mixed SnPb/SAC305 interconnections (Fig. 19) and likely reflects the effects of the different dissimilar microstructures and resulting mechanical properties. The middle and top solder ioints exhibited a preference for failure temperatures near the low end, not unlike the

SnPb/SAC305 test vehicles and according to the same, aforementioned reasons.

Mixed SnPb/SAC305 bottom interconnections; underfill, bottom gap, only.

The S/N09 and S/N10 test vehicles had mixed SnPb/SAC305 bottom solder joints. Underfill was placed only in the bottom gap. The bottom solder outperformed the top and middle interconnections. Thus, the event detection data were collected on only the top and middle solder which life-limiting ioints. were the interconnections of the PoPoP components in this configuration. A single data point was collected from the U10 component on S/N10 (4506 cycles) that confirmed the longer lifetimes of the bottom solder joints.

The log-log graph is shown in Fig. 23 that describes the cumulative failure fraction as a function of cycles to failure. The symbol colors designate the solder joint levels. The two data sets are nearly identical to one-another.

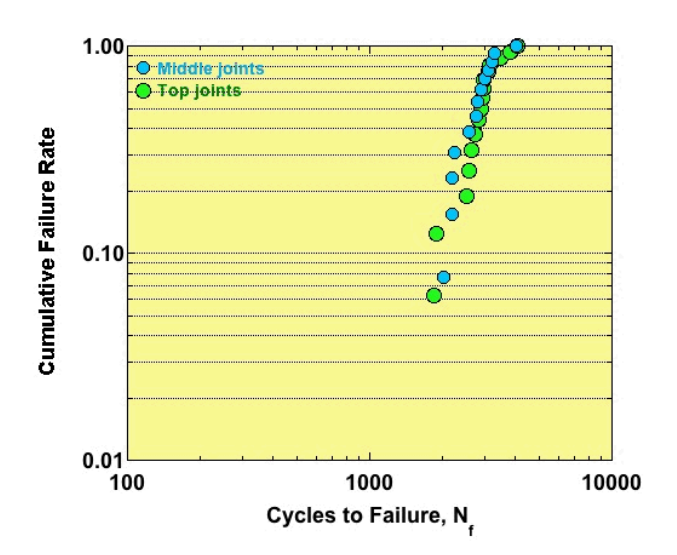


Figure 23. Log-log plot shows cumulative failure fraction as a function of cycles to failure for the top and middle solder joints from the test vehicles, S/N09 and S/N10. These PWAs had SnPb/SAC305 bottom interconnections and underfill was placed in the bottom gap.

The Weibull parameters are listed below for the individual top and middle solder joints as well as after having combined the two solder joint level together:

Top solder joints: $n = 3100\pm300$ eyeles: $\beta = 5.5\pm2.0$

Middle solder joints: $\eta = 3000\pm400 \text{ cycles}; \beta = 5.3\pm2.1$

Combined:

 $\eta = 3200\pm300 \text{ cycles}; \beta = 4.8\pm1.2$

As first indicated by Fig. 23, these Weibull parameters show that the top and bottom solder joints exhibited almost exactly the same TMF performance. Consequently, the combined case provides a suitable, single set of parameters to gate the overall reliability of the PoPoP components with underfill in the bottom gap.

These 2P Weibull parameters can be compared to those discussed above when underfill was not introduced into the gap. The corresponding Weibull parameters are listed in Table 2. The presence of the underfill increased the mean characteristic lifetimes of the top and middle interconnections. The underfill caused a slight increase in the η error terms so that, although there is a statistically significant difference between top interconnections, the middle solder joints have overlapping 95% confidence intervals that lessens the significance of improved reliability in the presence of underfill.

Table 2 2P Weibull Parameters of the SnPb/SAC305 Test Vehicles Representing the Cases of *No Underfill* and *Underfill*, *Bottom Gap Only*.

	No underfill		Underfill, bottom	
	η	β	η	β
Top solder joints	2600	8.7	3100	5.5
	<u>+</u> 200	± 4.0	<u>+</u> 300	<u>+</u> 2.1
Middle solder joints	2500	6.6	3000	5.3
	<u>+</u> 300	± 3.4	<u>+</u> 400	± 2.1
Bottom solder joints	2600	7.6	> 3500	
	<u>+</u> 200	± 3.5		

A similar improvement of TMF performance can be inferred for the bottom solder joints. This finding is based upon the preference for failures in middle and top solder joints as well as the single $N_{\rm f}$

data point (4506 cycles). This trend implies that the z-axis expansion of the underfill did not explicitly lessen the TMF reliability of the backwards compatible, bottom interconnections.

The data presented in Table 2 also show that the underfill reduced the β values of both top and middle interconnections to identical values. Relatively speaking, the decrease was greater for the top joints. Therefore, the introduction of underfill into the bottom gap widened the failure probability distribution for both top and middle solder joints, which raises the uncertainty for predicting failure in both rows of interconnections.

An important finding that is obtained from Table 2 is that placing underfill in the *bottom* gap has a synergistic effect on the TMF performance of both *top* and *middle* joints. Intuitively, it is reasonable to expect that the underfill would affect the middle solder joints due to their close proximity, but not the further removed, top solder joints. It was hypothesized that the underfill altered the contribution by warpage to the TMF performance of the top solder joints, resulting in the observed improvement to η .

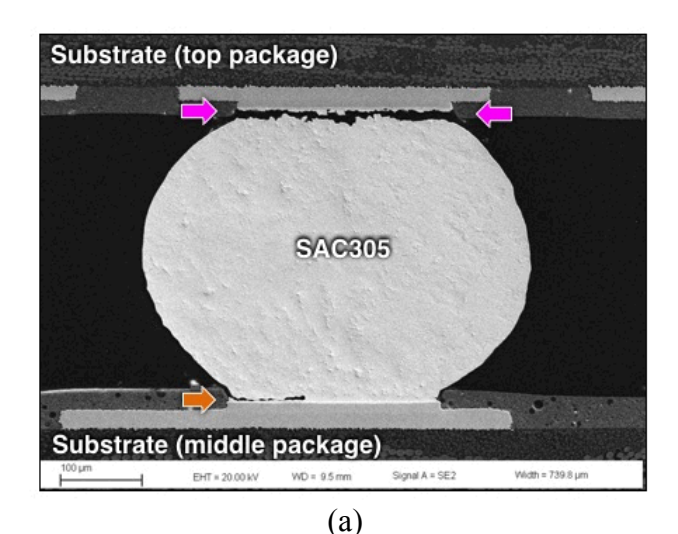
The failure modes were examined to substantiate the similarity of failure statistics between the top and middle solder joints as well as prolonged lifetimes of the bottom interconnections. The SEM photograph in Fig. 24a shows a top solder joint on the U10 PoPoP component from S/N10. The solder ball was completely separated from the pad of the top package substrate (magenta arrows). The crack morphology was commensurate with TMF crack behavior. A TMF crack had also initiated at the bottom of the joint (orange arrow).

The example of the middle solder joint is shown in Fig. 24b. The magenta arrows indicate the crack responsible for the electrical open (event). The orange arrow indicates the initiation of a crack at the top of the interconnections. Both the throughcracks and starter cracks had morphologies commensurate with TMF degradation.

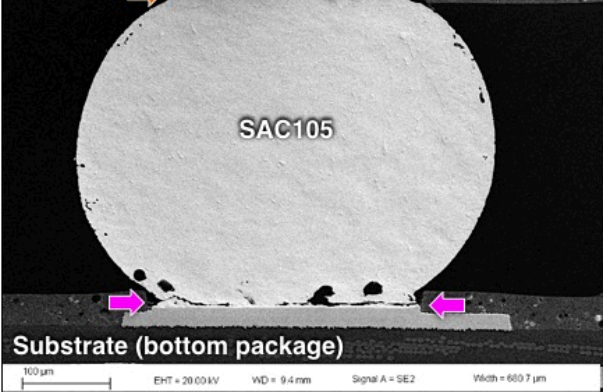
The SEM photograph in Fig. 24c shows the bottom solder joint. The BSE image mode was selected to

accentuate the homogeneous distribution of Pbrich phase throughout the microstructure. The light-blue arrows indicate accumulated Pbrich phase resulting from the growth of the Cu-Sn intermetallic compound (IMC) under exposure to the elevated temperature portion of the thermal cycle. The Pbrich layer is intermittent; when sufficient IMC layer growth causes the layer to be semi- or fully continuous, the solder joint can experience a loss of TMF resistance as that layer forms an easy path for crack propagation [6].

This image mode also highlights the underfill used to fill the gap. There is a small denuded that is typically observed at the top of the gap. The denuded zone is caused by a small amount of



Substrate (middle package)



Substrate (bottom package)

Cu-Sn IMC

Denuded zone

SnPb/SAC305

Underfill

Cu-Sn IMC

Cu pad

Solder mask

Printed circuit board

(c)

Figure 24. SEM photographs were taken of solder joints on the U10 component of S/N10 test vehicle, which represent the SnPb/SAC305 bottom joints and underfill in the bottom gap, only: (a) top solder joint; (b) middle solder joint; and (c) bottom solder joint.

settling by the filler particles after dispensing, but prior to the cure. The underfill remained adherent to the solder masks layer of both the PCB (below) and bottom package substrate (above).

Lastly, the plot was created in Fig. 25 that shows temperature at failure as a function of cycles to failure. Both the top and middle joints exhibited a largely random distribution of their respective N_f values across the temperature cycle range. This observation was contrary to the slight preference for failures to occur at the lower temperatures in the absence of underfill (Fig. 19). Since the underfill also experiences a loss of compliance at low temperature, this low-compliance mechanism, cannot, in-and-of-itself, cause the trends observed in Fig. 19 as was suggested in the earlier discussion. An indirect effect, specifically the warpage behavior, is a more viable cause of the trend in Fig. 19. However, the underfill mitigated that warpage effect according to the data in Fig 25.

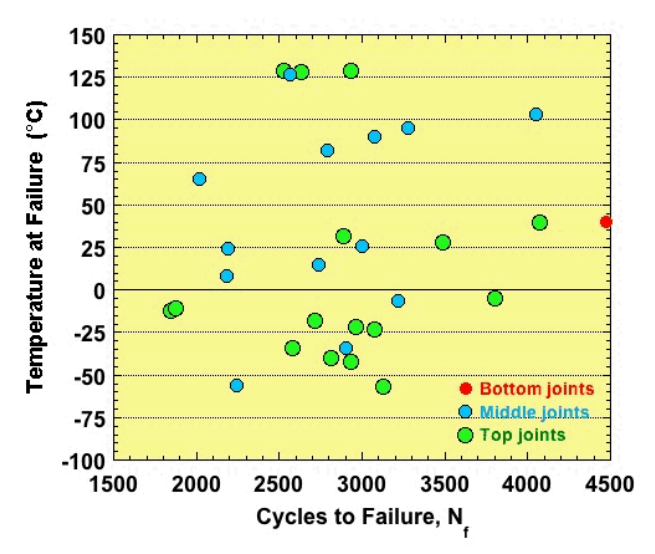


Figure 25. Temperature at failure was plotted as a function of cycles to failure (N_f) for the S/N09 and S/N10 test vehicles that represent the SnPb/SAC305 bottom interconnections and underfill only in the bottom gap.

100% SAC305 bottom interconnections; underfill, bottom gap, only.

The test vehicles were S/N33 and S/N36. The failure of the bottom, 100% SAC305 solder joints controlled the overall performance of the packages; as a result, only the failure data from those interconnections were collected for this case. The cumulative failure fraction is plotted as a function of cycles to failure in Fig. 26. The data had a wide distribution across N_f, that was accompanied by a knee in the curve at approximately a cumulative failure fraction value of 0.6 (1300 cycles mark). A knee in this plot traditionally indicates that two failure modes are active in the TMF failure regime.

The case of two failure mechanisms was further explored by dividing the data into two separate groups. One sub-group had a cumulative failure fraction of less than 0.6, and the second sub-group had a value of greater than 0.6. Then, a 2P Weibull analysis was performed on each sub-group, using the population size of that respective sub-group. Listed below are the 2P Weibull parameters for the bottom solder joints, first for the original, combined data set then after splitting out the failure results for two sub-groups:

Combined data set: $\eta = 1600\pm200 \text{ cycles}; \beta = 2.7\pm0.8$ CFF < 0.6: $\eta = 1000\pm100 \text{ cycles}; \beta = 6.3\pm2.5$ CFF > 0.6: $\eta = 2100\pm200 \text{ cycles}; \beta = 6.0\pm2.6$

The two sub-groups are described as "low η ", which had an η of 1000 cycles and "high η " that has an η of 2100 cycles. In spite of fewer data points, the error terms on the two η values were not significantly different from that of the combined data set.

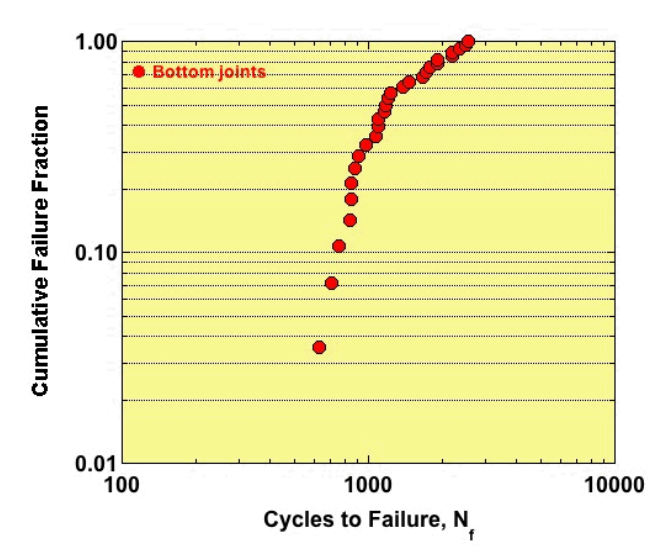


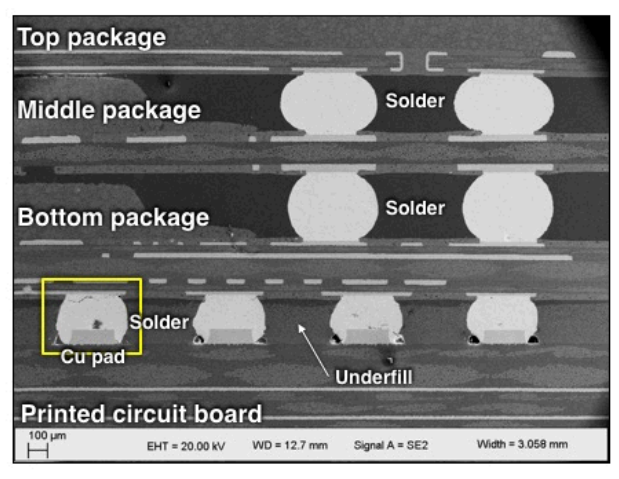
Figure 26. Log-log plot shows cumulative failure fraction as a function of cycles to failure for the bottom solder joints of S/N33 and S/N36. These test vehicles have 100% SAC305 bottom interconnections and underfill in the bottom gap, only.

Both sub-groups experienced higher slope (β) values than when combined, together. The increased β values imply that the separate sub-groups have tighter distributions than do the combined data set. This trend lends further confirmation that, in fact, the failure is characterized by two modes. The higher error terms observed with the sub-group β values will often accompany higher values of β because the steeper slope is more sensitive to the data spread than is a shallower slope.

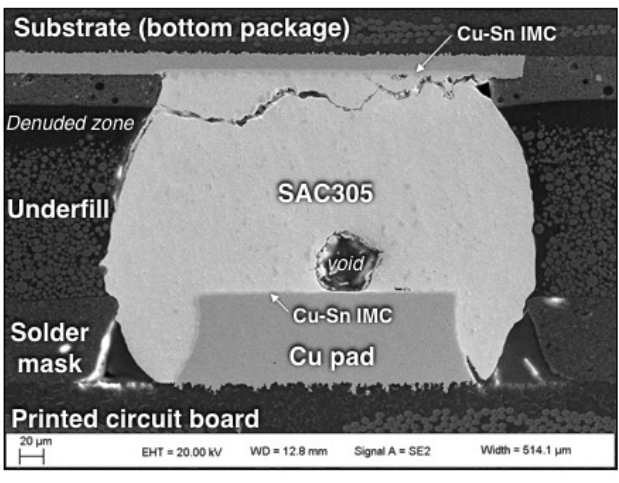
The circumstances of having two failure modes is that those PoPoP components having solder joints that failed by the "high η " mechanism avoided the "low η " mechanism. Given the fact that the "low η " sample size was 16 and the "high η " sub-group had a sample size of 12 implies that there is a significant probability that the PoPoP solder joints can be captured by the "low η " failure mode or by the "high η " failure mode. That is, the solder joints begin TMF with roughly an equal probability to experience *either* one *or* the other failure modes.

microstructures were examined components that represented the two sub-sets of TMF results. The "low η " case is discussed with reference to the SEM images in Fig. 27. The PoPoP test vehicle is S/N33 and the component is U14. An electrical open occurred after 704 cycles (125°C). The low magnification image of one side of section 1 is shown in Fig. 27a. The individual package structures, underfill, and PCB structures did not experience any damage. As indicated by the failure data, the bottom solder joints experienced the TMF cracking responsible for the package failure. Aside from the distortion owed to warpage, the top and middle solder joints did not exhibit TMF cracking or other degradation artifacts. The high magnification SEM image is shown in Fig. 27b of the solder joint outlined by the yellow box in Fig. 27a. A through crack is observed near the top of the interconnection that has a morphology indicative of TMF.

The analysis turned to the U01 component S/N33 test vehicle. This PoPoP device represented the "high η " sub-set; it failed after 1779 cycles (125°C). The low magnification SEM image is shown in Fig. 28a of one side of section 1 from the U10 component. Significant TMF deformation was observed on the bottom interconnections, which corroborates the failure data that these interconnections controlled the PoPoP failure behavior. An unusual crack development was observed at the PCB side of the bottom interconnections (red arrows). The morphology of these cracks did not have the general characteristics of TMF cracking, (e.g., Fig. 27).



(a)

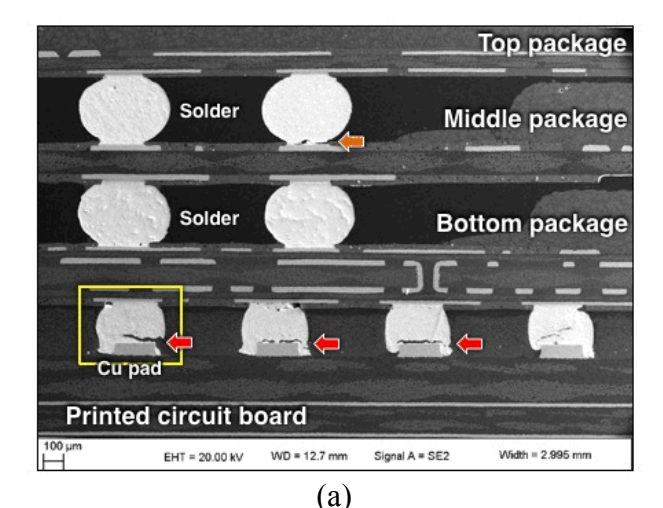


(b)

Figure 27. SEM photographs were taken of solder joints on the U14 component of the S/N33 test vehicle, which represent the "low η " case of 100%SAC305 bottom joints and underfill only in the bottom gap: (a) low magnification photograph of one side of section 1 and (b) high magnification image of the bottom solder joint identified by the yellow box in (a).

A high magnification, SEM image is shown in Fig. 28b that is representative of the bottom interconnections (yellow box in Fig. 28a). A TMF crack appears at the top of the joint, which was responsible for the electrical open. The additional crack is identified by the red arrows at the bottom of the joint. The morphology of the defect indicated that it was the result of a *tensile load*. A review of the other solder joints in Fig. 28a, as well as those from the remaining cross sections, also indicated a morphology that is characteristic of

tensile fracture. Past modeling studies have confirmed that the presence of underfill in the bottom gap had a limited effect on the degree of warpage between the PoPoP component and the PCB [5]. Therefore, warpage did not appear to be the likely source of the tensile load.



Substrate (bottom package)

Cu-Sn IMC

Missing solder material

Solder mask

Cu-Sn IMC

Cu pad

Printed circuit board

20 µm

EHT = 20.00 kV WD = 12.8 mm Signal A = SE2 Width = 514.1 µm

Figure 28. SEM photographs were taken of solder joints on the U01 component of the S/N33 test vehicle, which represent the "high η " case of 100%SAC305 bottom joints and underfill only in the bottom gap: (a) Low magnification photograph shows one side of section 1. The red arrows indicate an additional crack behavior in the solder joints. (b) High magnification image was taken of the bottom interconnection identified by the yellow box in (a). The red arrows highlight the additional crack.

(b)

The analysis considered other effects of the underfill material. The underfill has a z-axis

coefficient of thermal expansion (CTE) equal to 23 ppm/ $^{\circ}$ C when below its glass transition temperature (T_g) of 120 $^{\circ}$ C. This value is very closely matched to that of the 100% SAC305 solder material. However, when T_g is exceeded, the CTE climbs to 85 ppm/ $^{\circ}$ C. Since the accelerated aging temperature cycle has a maximum temperature of 125 $^{\circ}$ C, it is very likely that the change between low and high CTE values as the underfill passed through it glass transition generated an additional tensile load on the joints that gave rise to the tensile crack observed in Fig. 28.

Several observations remain to be explained vis-avis the theory that a high CTE by the underfill resulted in the tensile cracks of these solder joints. First and foremost, this behavior is associated with test vehicles that actually exhibited longer characteristic lifetimes ("high η "). The presence of additional degradation leading to a longer TMF lifetimes seems counterintuitive. However, a plausible scenario was developed to explain this behavior. The process begins with the formation of the tensile cracks in the first "few" cycles ("few" can be several tens or hundreds). The TMF strain, which is responsible for the subsequent electrical failure, is reduced by those pre-existing tensile cracks. The net result is that more cycles are required to propagate the TMF crack, which is ultimately responsible for the solder joint failure. This scenario is supported by the fact that (a) the tensile cracks did not create an electrical open and (b) the TMF crack and tensile cracks occurred at different locations in the solder joint.

A second observation was that the tensile cracks and associated improvement in fatigue life occurred on only 43% of these test vehicles. The temperature cycle overlapped the glass transition "range" of the underfill. Glass transition is a second-order phase change and, as such, does not occur at a single temperature; rather, it takes place over a small range of temperatures. This fact, coupled with a complicated strain state caused by the complex structure of the PoPoP as well as the stochastic nature of the cracking behavior, itself, placed this behavior at "the edge of cliff." The PoPoP bottom solder joint had an approximately

even probability of exhibiting the "low η " or "high η " failure mode.

The third and final observation was that the tensile cracks and bi-modal cumulative failure distribution was not observed for the test vehicles having the mixed SnPb/SAC305 bottom solder joints and underfill in the bottom gap (test vehicles S/N09 and 10). Recall that only the middle and top solder joints had their failure statistics analyzed against the 2P Weibull distribution. The SnPb/SAC305 bottom interconnections outlived the former solder (A lower limit to their characteristic ioints. was approximately 3200 lifetimes cycles.) Referring to Table 1, in the absence of an underfill, the SnPb/SAC305 and 100%SAC joints exhibited similar TMF reliability. Therefore, based on this similarity, the SnPb/SAC305 joints would be predicted to have an η of 1000 - 2100 cycles, which is *not* the case. This analysis, when combined with the absence of tensile cracks in the solder (see Fig. 24c), support the inference that the bimodal failure behavior observed in Fig. 26 did not occur with the backwards compatible interconnections. Therefore, the occurrence of the tensile crack phenomenon is unique to the 100% SAC305 microstructure and, as such, mechanical properties of the solder composition comprising the bottom interconnections. In terms of PoPoP reliability, the mixed SnPb/SAC305 interconnections exhibited better TMF behavior over their 100% SAC305 counterparts in the presence of underfill in the bottom gap.

The last analysis of the S/N33 and S/N36 test vehicles addressed the temperature at failure as a function of cycles to failure (N_f). The corresponding plot is shown in Fig. 29. Of the twenty-eight daisy chains that monitored the bottom joints, twenty-five of them (89%) had an electrical failure at the maximum temperature of 125°C. It was noted earlier that the preference for failures to occur at the high temperatures suggests that z-axis expansion of the underfill contributes. significantly, to the TMF deformation of the solder ioints. This premise applies to the present interconnections, particularly given that the failure includes tensile cracks (Fig. Additionally, only 43% of the daisy chains were in

the "high η " sub-set and, by inference, exhibited the tensile crack development. However, the data in Fig. 29 indicates that the underlying underfill expansion mechanism was present in nearly all of the PoPoP components. This discrepancy confirmed the "edge of the cliff" condition and with it, the stochastic nature behind formation the tensile crack initiation.

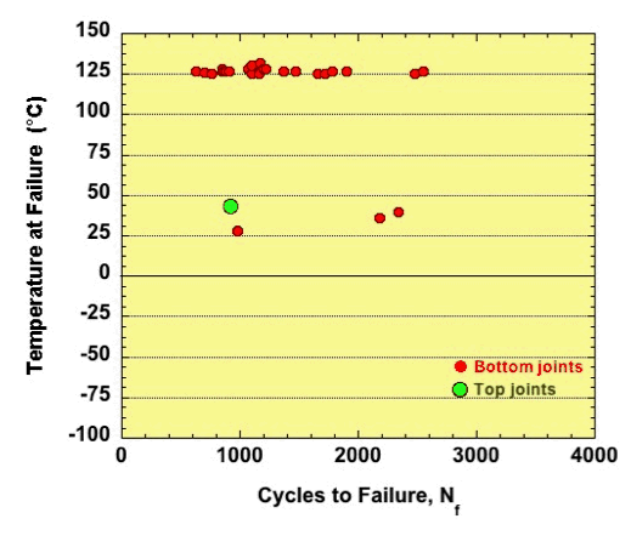


Figure 29. Temperature at failure was plotted as a function of cycles to failure (N_f) for the S/N33 and S/N36 test vehicles that represent the 100% SAC305 bottom interconnections and underfill only in the bottom gap.

Computational model

Finite element constructs

The development of the computation model that predicts the TMF of the solder interconnections began with the construction of the finite element representations of the PoPoP package variants. The geometric dimensions were determined from drawings and metallographic cross sections made of the test vehicles. Next, the optimum symmetry was developed, which included critical geometric features, but at the same time, minimized computational time. This step is illustrated in Fig. 30. Underfill was placed in all gaps of this solid model to better illustrate the structure. The onehalf symmetry is shown by the (a) solid model. A cross section view is provided in (b) of one side of the solder joint stack. The solid model is shown in (c) that represent the one-eighth symmetry, which was used in the numerical computations. build-up of the PoPoP assembly in one-eighth

symmetry (without underfill) is shown by the sequence of solid models in Fig. 31: (a) bottom solder joints and the PCB; (b) bottom package and middle solder joints; (c) bottom and middle packages plus the top solder joints; and (d) addition of the top package to complete the PoPoP.

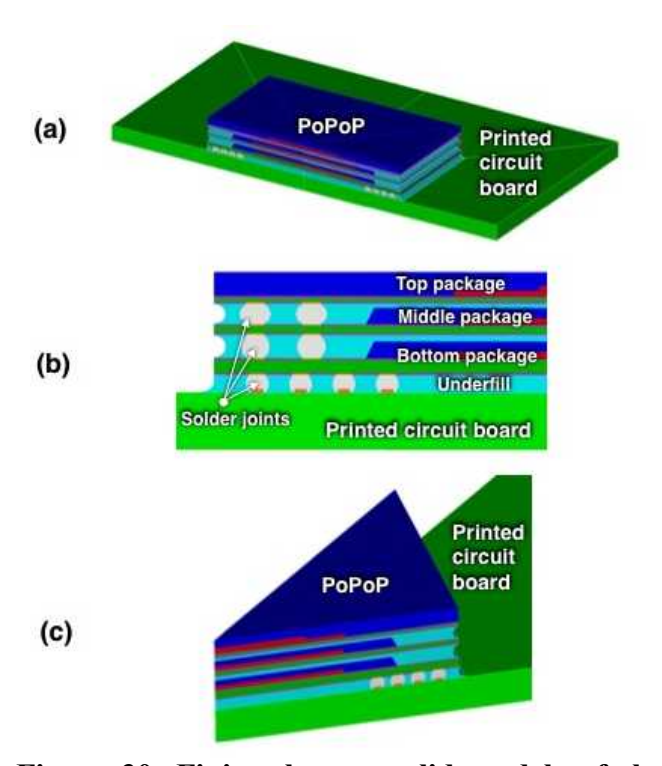


Figure 30. Finite element solid models of the PoPoP assembly. Underfill was placed in all of the gaps for visualization purposes. (a) One-half symmetry provides a cross section view of across the PoPoP component and solder interconnections. (b) Magnified view shows one side of the cross section. (c) Solid model shows the one-eighth symmetry cut that was used in the numerical computations.

The computation of TMF in the solder joints begins with the unified creep-plasticity equation (UCP) [7, 8]. The model contains the elastic and inelastic responses of the materials comprising the structures: individual package molding compound, underfill, substrates, PCB, and solder alloys. Lastly, the temperature cycling conditions are added to the numerical code. The model is executed, the output of which, is a deterministic (non-statistical) prediction of TMF deformation and crack development in the solder joints.

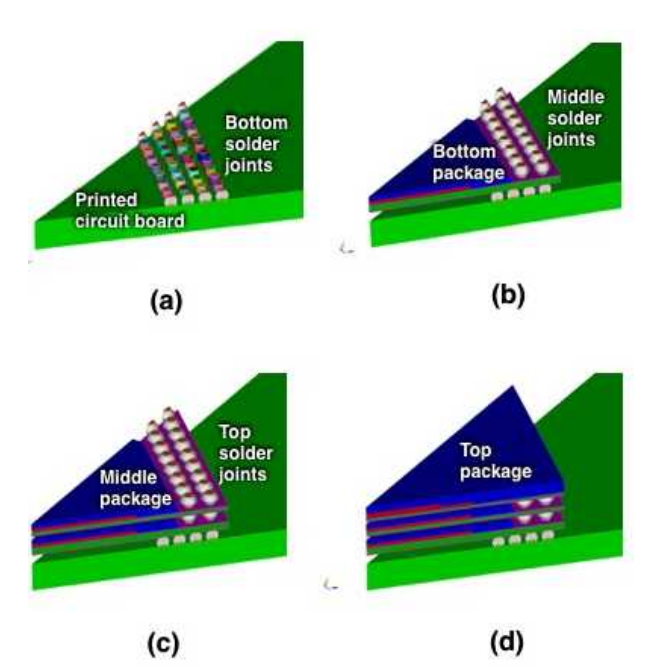


Figure 31. One-eighth symmetry solid models show the build-up of the PoPoP assembly in the sequence of (a) to (d).

Warpage predictions

The first analysis was made of the extent of warpage that occurs to the PoPoP/PCB assembly. The solid model cross sections are shown in Fig. 32. The displacements have been magnified by 20x. The bottom solder joints were the 100% SAC305 interconnections: the extent of warpage is relatively insensitive to solder composition. The two cases illustrated in Fig. 32 were "no underfill" and "underfill, bottom, only." Warpage was predicted at the temperature limits of -55°C, and 125°C. The "zero" warpage state was placed at 25°C as an accounting was not made of cool down from the soldering temperature or underfill curing temperature at this juncture. (Recall that warpage was clearly observed at 25°C.) The objective of this abbreviated analysis was to make a first-order comparison of relative displacements between the underfill variants.

The warpage analysis of the PoPoP components was addressed as strictly as a mechanics problem. Solder joint creep was not applied to the problem. The degree of warpage can be visualized, based upon the dashed lines that provide both positional data as well as a constant separation distance (z_0) to measure z-axis expansion and contraction.

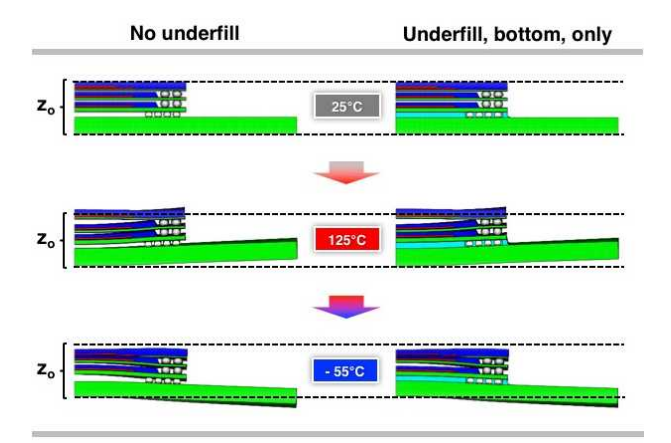


Figure 32. Solid model "cross sections" show the extent of warpage at 25°C, 125°C, and -55°C for PoPoP assemblies having no underfill and the case of underfill present only in the bottom gap. The dashed lines provide visual references; z_0 is held constant across all of the images.

The analysis of Fig. 32 brought about several findings. As expected from the relative CTE values of the package constructs and PCB. "smiley-face" warpage is predicted at 125°C; it becomes "frowny-face" warpage at -55°C. Byand-large, the solid models in Fig. 32 predict that warpage would not change significantly with the addition of underfill to the bottom gap. observation confirms that the change to the TMF performance of the bottom interconnections resulting from the introduction of underfill improvement for the SnPb/SAC305 joints and degradation to 100% SAC305 joints – was unlikely to have been affected by the warpage behavior of the PoPoP assembly. Rather, the opposing trends reflect strictly the susceptibility of the respective solder joint metallurgies to the tensile loads generated by the higher, z-axis CTE of the underfill when the latter either wholly or partially passed through its glass transition zone when the thermal cycle approached the maximum temperature.

Although the failure data are not presented here for the case of underfill in two or all three of the gaps, the solid models were generated to predict the warpage behavior. Those results are shown in Fig. 33. The magnitude of the z-axis expansion and contraction between the top package and PCB is of the same order-of-magnitude as the degree of warpage. This observation underscores the contributing role of z-axis expansion on the TMF of the solder joints as exemplified by Fig. 28b

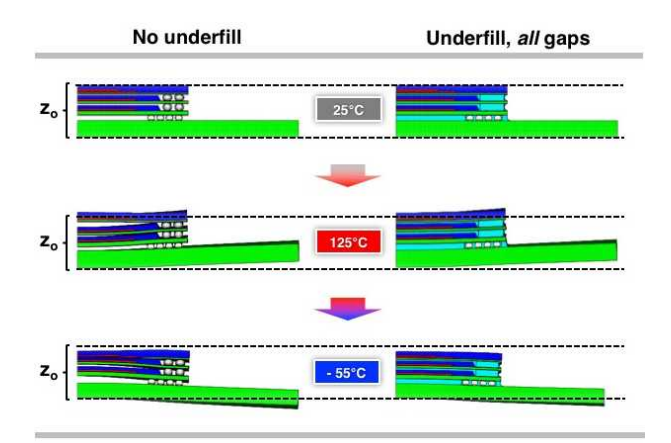


Figure 33. Solid model "cross sections" show the extent of warpage at 25°C, 125°C, and -55°C for PoPoP assemblies having no underfill and those having underfill in *all* of the gaps. The dashed lines provide visual references; z_0 is held constant for all of the images.

TMF predictions

The computational model was exercised to generate predictions of the cycles to reach crack initiation and 100% failure of the solder joints (electrical open). The latter predictions would be validated against the empirical data discussed above. The first set of model outputs were significantly off-the-mark. Discrepancies were observed when the step was taken to validate the predicted cycles against the empirical N_f values as well as trends as a function of underfill in the bottom gap.

The poor validation outcome led to a systematic assessment of the effect of materials properties and geometries assigned to the PoPoP and PCB structures. The first revision to the model brought the predicted cycles-to-failure to within a factor of two (2) of the N_f data. Unfortunately, the trends predicted between the two underfill variants did not corroborate the experimental observations.

It became clear, very quickly, that the static mechanics problem could be readily solved by the model so as to predict behaviors such as warpage (Figs., 32 and 33). However, the high complexity of the PoPoP assembly, and the synergistic effects

of both materials properties and geometries, would require that greater scrutiny be given to the development of the computational model in order for the latter to accurately predict solder joint TMF over the several *thousands* of cycles required to reach failure

CONCLUSIONS

- 1. A long-term reliability program is underway to assess the feasibility of stacked packages for use in high-reliability military, space, and satellite electronics. The present study examined the TMF performance of PoPoP assemblies tested under accelerated aging (-55°C/125°C experiments temperature cycling). The development of a computational model is included in this effort to predict the **TMF** of all three levels ofsolder interconnections.
- 2. Empirical failure event data were analyzed by the two-parameter (2P) Weibull probability distribution (characteristic lifetime, η , and slope, β). A detailed, failure mode analysis accompanied the quantitative evaluations.
- 3. The test vehicles included variants of bottom solder joints backwards compatible mixed SnPb/SAC305 versus 100% SAC305 Pb-free joints as well as the placement of underfill in the gaps bottom, only; bottom and middle gaps; as well as bottom, middle, and top gaps.
- 4. Aside from a single test vehicle, all of the other SnPb/SAC305 solder joints exhibited the homogeneous microstructure that results from complete mixing of the two solders.
- 5. The test vehicles having the backwards compatible, bottom solder joints exhibited excellent TMF performance for, not only those interconnections ($\eta = 2600\pm200$ cycles; $\beta = 7.6\pm3.5$), but also for the middle joints ($\eta = 2500\pm300$ cycles; $\beta = 6.6\pm3.4$) and top interconnections ($\eta = 2600\pm200$ cycles; $\beta = 8.7\pm4.0$).
- The test vehicles having 100% SAC305 bottom solder joints exhibited Weibull parameters that were comparable to those of the mixed solder joints to within experimental error. Characteristic lifetimes (η) were: bottom,

- 2200±200 cycles; middle, 2600±500 cycles; and top, 2400±200 cycles.
- 7. The introduction of underfill to the bottom solder joints *improved* the characteristic lifetimes of all interconnections on the SnPb/SAC305 test vehicle. The failure data exhibited slightly lower slope parameters.
- 8. The test vehicles having 100% SAC305 bottom solder joints exhibited a degradation to those interconnections with the addition of underfill in the corresponding gap. Moreover, the empirical statistics indicated *two* failure modes: a "low η" sub-set that exhibited the typical TMF crack development and a "high η" sub-set that exhibited both TMF and tensile cracks in the solder joint.
- 9. The tensile cracks, which *improved* reliability against TMF, were generated by the thermal expansion of the underfill. This hypothesis was corroborated by the temperature-at-failure data.
- 10. The computational model, when used to predict static mechanical behavior, showed that PoPoP warpage was not significantly changed by the presence of underfill in the bottom gap. Z-axis thermal expansion displacements were of a comparable magnitude to the warpage magnitudes. A validation of the initial, quantitative predictions of N_f indicated the for further development the PoPoP model to realize the fidelity required for the latter to serve as a design tool of this technology.

REFERENCES

- [1] P. Vianco, "Processing and Reliability of Solder Interconnections in Stacked Packaging," to be published in *3D Microelectronic. Packaging: From Fundamentals to Applications*, eds. Y. Li and D. Goyal (Springer, 2016).
- [2] R. Johnson, M. Strickland., and D. Gerke: "3-D Packaging: A Technology Review" *NASA Tech. Rep 20050215652* (NASA MSFC Huntsville, AL; 2005).
- [3] R. Priori and A. Burton: "Development of a High Reliability and Large Volume Manufacturing Assembly Process for a Stacked Memory Package.

Proc. IEEE Elect. Comp. and Tech. Conf. (IEEE, New York, NY, June 2004) 1142 – 1147.

- [4] P. Vianco, J. Grazier, J. Rejent, A. Kilgo, F. Verdi, and C. Meola, "Temperature Cycling of Pb-Free and Mixed Solder Interconnections Used on a Package-on-Package Test Vehicle," *Proc. Surf. Mount. Tech. Assoc. Inter.* (SMTA, Edina, MN: 2009) CD-ROM.
- [5] P. Vianco, M. Neilsen, J. Rejent, J. Grazier, and A. Kilgo, "Predicting the Reliability of Package-on-Package Interconnections Using Computational Modeling Software," *Proc. Surface Mount Tech. Assoc. Inter.* 2015 (SMTA, Edina, MN; 2013) CD-ROM.
- [6] P. Vianco, J. Rejent, J. Grazier, S. Garrett, S. Sokolowski, G. Dinger, M. Neilsen, L. Halbleib, A. Kilgo, and R. Grant, "Qualification Program for the Solder Interconnections of Three Area-Array Packages on Copper and Non-Copper Core, Multi-Layered Printed Circuit Boards," *Sandia Report* SAND2015-7495 (Sandia National Laboratories, Albuquerque, NM; 2015).
- [7] A. Fossum, P. Vianco, M. Neilsen, and D. Pierce, "A Practical Viscoplastic Damage Model for Lead-Free Solder, " *Journal of Electronic Packaging* 128 (2006), 71 81.
- [8] M. Neilsen and P. Vianco, "UCPD Model for Pb-free Solder, *Journal Electronic Packaging* Dec. 2014 DOI: 10.1115/1.4026851.

ACKNOWLEDGEMENT

The authors wish to thank Mark McKewen of STI Electronics for his supervision of the assembly of the test vehicles. Also, we wish to show our gratitude to Brian Wroblewski for his careful review of the manuscript. Sandia is a multiprogram laboratory operated by Sandia Corporation, a Lockheed Martin Company, for the United States Department of Energy's National Nuclear Security Administration under Contract No. DE-AC04-94AL85000.